

Meson properties in an extended nonlocal NJL model

Robert S. Plant and Michael C. Birse

Theoretical Physics Group, Department of Physics and Astronomy,

University of Manchester, Manchester, M13 9PL, U.K.

We consider a nonlocal version of the NJL model, based on a separable quark-quark interaction. The interaction is extended to include terms that bind vector and axial-vector mesons. The nonlocality means that no further regulator is required. Moreover the model is able to confine the quarks by generating a quark propagator without poles at real energies. Working in the ladder approximation, we calculate amplitudes in Euclidean space and discuss features of their continuation to Minkowski energies. Conserved currents are constructed and we demonstrate their consistency with various Ward identities. Various meson masses are calculated, along with their strong and electromagnetic decay amplitudes. We also calculate the electromagnetic form factor of the pion, as well as form factors associated with the processes $\gamma\gamma^* \rightarrow \pi^0$ and $\omega \rightarrow \pi^0\gamma^*$. The results are found to lead to a satisfactory phenomenology and lend some dynamical support to the idea of vector-meson dominance.

I. INTRODUCTION

The Nambu–Jona-Lasinio (NJL) model [1–3] has long been used as a starting point for the description of light mesonic states as fermion-antifermion composites. It shares several features with QCD, notably a dynamically-broken chiral symmetry, with the pions as approximate Goldstone bosons. The model is based on fermionic fields interacting through

a local, chirally-invariant, four-point vertex. The local nature of the interaction produces a great simplification of the Schwinger–Dyson and Bethe–Salpeter equations. The main drawbacks of the model are, however, direct consequences of this locality. Specifically, they are that the loop integrals diverge (and so must somehow be regulated) and that the model is non-confining.

Although the NJL model does contain regularization-independent information [4,5] and the results with various regularization schemes have been found to be qualitatively similar [6], the choice of any particular scheme lacks a sound physical motivation. A feature of many regularization schemes is that as well as the form of the cut-off, a particular momentum routing must be specified for loop diagrams with two-or-more quark lines [7]. In practice a symmetric routing is often implicitly taken in order to maintain Ward identities. The regularization scheme must be specified yet further if one wishes to calculate beyond leading order in the $1/N_c$ expansion, a new cut-off being required for meson loops [8].

Another unsatisfactory aspect is that if low-energy theorems for anomalous processes (for example $\pi^0 \rightarrow \gamma\gamma$) are to hold then the anomalous diagrams must either be left unregulated [9] or else additional terms must be added to the Lagrangian in order to respect the anomalous Ward identities [5]. Related problems occur in the presence of vector interactions [9–12] if one attempts to apply the regularization prescription to both the anomalous and non-anomalous sectors.

Many attempts have been made to generalize the original NJL model [13] to remove such unwanted features whilst retaining its successful phenomenological aspects [2,3]. One promising approach, which provides some motivation for the model studied here, is suggested by instanton-liquid studies [14]. In that picture, the instantons induce an effective four-quark vertex, which is nonlocal but of a separable form. The separable nature of the interaction retains as far as possible the simplifying features of a local model, with the non-locality providing a cut-off on all loop integrals. A similar class of model has a separable dependence on the relative momentum of the $\bar{q}q$ pair and has been studied in Refs. [15,16]. Other models with simple interactions have been suggested based on various types of glu-

onic field configurations within the QCD vacuum. For example, Efimov and coworkers [17] start with a constant (anti-) self-dual background field in Euclidean space and base their four-quark vertex on one-gluon exchange within such a background. Yet another recent model [18] used a four-quark vertex mediated by a random colour-matrix, as an attempt to simulate a strongly-fluctuating background gluon field (see also [19]). We should mention that there are also studies of QCD Schwinger–Dyson equations based on one-gluon exchange forces between the quarks, often using effective gluon propagators [20,21] (also see [22] and references therein).

Here we develop further the model proposed in Ref. [23]. This is based on a nonlocal, separable, four-quark vertex. It is therefore similar to the instanton-liquid model of Ref. [14], the differences being that more general choices of the form factor and possible couplings are considered. The particular choice of form factor used in this model can lead to quark confinement, in the sense of a quark propagator without poles at real energies. It also ensures convergence of the quark-loop integrals, unlike that chosen in the separable model of Ref. [24]. Only the pions and their scalar partner were studied in Ref. [23]. In the spirit of the extended NJL model [3–5,9,25–28], we incorporate other mesonic degrees of freedom, such as the vector mesons. Including these particles enables us to probe the role of the confinement mechanism, since they have masses of around twice a typical constituent-quark mass. In a model without confinement, and with an otherwise reasonable constituent-quark mass of ~ 300 MeV, the ρ meson would lie above the $\bar{q}q$ threshold and could decay into free $\bar{q}q$ states.

As well as the meson spectrum, we calculate hadronic decays of these particles and some electromagnetic processes, including $\rho \rightarrow e^+e^-$ and the pion form factor, all at leading order in the $1/N_c$ expansion. With regard to the electromagnetic processes, we also examine whether there is any support for the concept of vector-meson dominance within a model of this type.

This paper is organized as follows. In Sec. II we define the extended model and give the forms of the corresponding vector and axial currents. In Sec. III we present the forms of the

quark and meson propagators and describe the means of coupling to external currents. The determination of the model parameters is described in Sec. IV, and results for hadronic and electromagnetic decays of mesons are present in Secs. V and VI respectively.

II. THE MODEL

Formally at least, one can imagine integrating out gluonic degrees of freedom to leave an effective action for QCD expressed in terms of quark fields only. As in the usual NJL model, we keep only two-body forces between the quarks, described by four-quark interaction vertices. Indeed, at leading order in $1/N_c$, all six-quark and higher interactions could be absorbed into effective couplings for the four-quark terms, by replacing extra $\bar{\psi}\Gamma\psi$ factors with their vacuum expectation values. This is just the procedure followed in the three-flavour extended NJL model [27,28] with a six-quark, $U(1)_A$ -breaking 't Hooft determinant [29]. In the present work, however, we specialize to two-flavours with isospin symmetry. The action may be written as

$$S = \int d^4x \bar{\psi}(x)(i\partial - m_c)\psi(x) + \sum_i \int \prod_n d^4x_n H_i(x_1, x_2, x_3, x_4) \bar{\psi}(x_1)\Gamma_i^\alpha\psi(x_3)\bar{\psi}(x_2)\Gamma_{i\alpha}\psi(x_4). \quad (1)$$

Imposing $SU(2)_V \times SU(2)_A \times U(1)_V$ symmetry requires that certain of the possible Dirac and isospin structures appear in the combinations:

$$\begin{aligned} H_1(1 \otimes 1 + i\gamma_5\tau^a \otimes i\gamma_5\tau^a), \quad & H_2(\gamma^\mu\tau^a \otimes \gamma_\mu\tau^a + \gamma^\mu\gamma_5\tau^a \otimes \gamma_\mu\gamma_5\tau^a), \\ H_5(\tau^a \otimes \tau^a + i\gamma_5 \otimes i\gamma_5), \quad & H_6(\sigma_{\mu\nu} \otimes \sigma^{\mu\nu} - \sigma_{\mu\nu}\tau^a \otimes \sigma^{\mu\nu}\tau^a), \end{aligned} \quad (2)$$

whilst the strengths of the following interactions are unconstrained by symmetry considerations:

$$H_3(\gamma^\mu \otimes \gamma_\mu), \quad H_4(\gamma^\mu\gamma_5 \otimes \gamma_\mu\gamma_5). \quad (3)$$

A variety of models of the above type can be found in the literature, differing in the ansatz chosen for $\{H_i(x_1, x_2, x_3, x_4)\}$. The original NJL model, for instance, has $H_1 \sim$

$\int d^4x \prod_n \delta(x - x_n)$ and a constant coupling strength, whereas one-gluon exchange models take $H_i \sim \delta(x_1 - x_3)\delta(x_2 - x_4)D(x_1 - x_2)$. Our own approach is motivated in part by the instanton-liquid model [14]. Within the zero-mode approximation to that picture, there is a $2N_f$ -quark interaction, which is of separable form,

$$H_i(p_1, p_2, p_3, p_4) = \frac{1}{2}(2\pi)^4 G_i f(p_1) f(p_2) f(p_3) f(p_4) \delta(p_1 + p_2 - p_3 - p_4). \quad (4)$$

In the model of Ref. [14] the function $f(p)$ is of a particular form and for two flavours of quarks the relation $G_1 = -G_5$ follows from the form of the 't Hooft determinant [29]. An interaction of tensor character is also present but is $1/N_c$ suppressed.

The model studied here is similar to that of Dyakonov and Petrov [14], in that it is based on an interaction with the separable form (4). However, we shall adopt a more phenomenological attitude towards the form-factor $f(p)$ and the allowed couplings. Only interactions in the colour-singlet channels are considered in the present study. The G_1 coupling (in the ladder approximation) produces the pions and their isoscalar scalar partner, σ . The couplings in the spin-1 channels G_2 , G_3 and G_4 are responsible for the ρ , a_1 , ω and f_1 mesons. The G_5 coupling allows the model to describe an isovector scalar and an isoscalar pseudoscalar meson. The lowest-lying meson with quantum numbers corresponding to the former is $a_0(980)$, whilst the latter is a non-strange state with the quantum numbers of the η and η' , which we shall refer to as η^* .

We shall not consider the possible tensor interactions, described by the coupling G_6 . As discussed in Ref. [27], these can contribute in the vector channels, where they give rise to anomalous magnetic-moment couplings of the vector mesons to constituent quarks. In the absence of any strong phenomenological need for such couplings we choose not to include them.

For the sake of simplicity, all of the possible independent interactions (2,3) are assumed to contain the same form factor and to differ only in the constant coupling strengths, G_i . As in Ref. [23], we take the form factor to be Gaussian in Euclidean space:

$$f(p_E) = \exp(-p_E^2/\Lambda^2). \quad (5)$$

This choice was shown to be able to give quark confinement. We have in fact examined the possibility of taking a different Λ for each of the independent couplings. Since this does not lead to any very significant effects, the results are not presented here. This is because the main features are dominated by the form of the quark self-energy which, in the ladder approximation, depends only on the G_1 interaction.

The usual, local expressions for the vector and axial currents do not satisfy the correct continuity equations when one uses the equations of motion derived from the action (1–4). In order to obtain symmetry currents with the same divergences as the corresponding local currents in QCD, and hence to maintain the corresponding Ward identities, one has to introduce additional nonlocal terms in the currents. A Noether-like method of construction for these nonlocal pieces was developed in Ref. [23]. As a part of that procedure the following identity was used,

$$\delta(x - x_1) - \delta(x - x_2) = \int_0^1 d\lambda \frac{dz^\mu}{d\lambda} \partial_\mu \delta(x - z), \quad (6)$$

$z(\lambda)$ being some arbitrary path from x_1 to x_2 . The divergence requirement determines the longitudinal component of a current which is, therefore, a path-independent object. In Ref. [23] the choice of path was irrelevant since the authors were interested only in the longitudinal component of the axial current, in order to determine the pion decay constant. The transverse part of the current, however, is sensitive to the particular choice of $z(\lambda)$. Indeed, ambiguity in the transverse current is a feature of any method used to construct a (partially) conserved current corresponding to a nonlocal action. When one wishes to consider electromagnetic processes, as in the present work, it is necessary to assume some form for the transverse current. This assumption forms an additional part of the specification of the model. In our present calculations, we adopt the straight line ansatz [23],

$$z(\lambda) = (1 - \lambda)x_1 + \lambda x_2, \quad (7)$$

being the simplest choice available.

The nonlocal interactions in the model defined by (1–4) give rise to various nonlocal terms in the currents, whose momentum-space forms are presented below. (Note that where

momentum derivatives with respect to $p_i \pm p_j$ occur, then the combination $p_i \mp p_j$ is understood to be held fixed.) For the isoscalar vector current, the nonlocal pieces all have the structure,

$$J_{(I)}^\mu = \frac{1}{(2\pi)^{12}} \sum_i G_i \int \prod_n d^4 p_n \bar{\psi}(p_1) \Gamma_i^\alpha \psi(p_3) \bar{\psi}(p_2) \Omega_{i\alpha} \psi(p_4) \delta(p_1 + p_2 + q - p_3 - p_4) \times \int_0^1 d\lambda f(p_2) f(p_4) \frac{\partial}{\partial(p_1 + p_3)_\mu} f(p_1 + \lambda q) f(p_3 - q + \lambda q), \quad (8)$$

which we refer to as type I. The sum over $G_i(\Gamma_i^\alpha \otimes \Omega_{i\alpha})$ in (8) runs over the same combinations of couplings and Dirac and isospin matrices as those found in the action, (2,3).

The isovector vector current also has nonlocal contributions of this type-I structure (8). In this case the isospin and Dirac matrices appear in the combinations:

$$G_1(\tau^a \otimes 1 + i\gamma_5 \otimes i\gamma_5 \tau^a), \quad G_2(\gamma^\nu \otimes \gamma_\nu \tau^a + \gamma^\nu \gamma_5 \otimes \gamma_\nu \gamma_5 \tau^a), \\ G_3(\gamma^\nu \tau^a \otimes \gamma_\nu), \quad G_4(\gamma^\nu \gamma_5 \tau^a \otimes \gamma_\nu \gamma_5), \quad G_5(1 \otimes \tau^a + i\gamma_5 \tau^a \otimes i\gamma_5). \quad (9)$$

Another type of nonlocal structure also arises in this current,

$$J_{(II)}^\mu = \frac{i\epsilon^{abc}}{2(2\pi)^{12}} \sum_i G_i \int \prod_n d^4 p_n \bar{\psi}(p_1) \Gamma_i^a \tau^b \psi(p_3) \bar{\psi}(p_2) \Omega_{i\alpha} \tau^c \psi(p_4) \delta(p_1 + p_2 + q - p_3 - p_4) \times \int_0^1 d\lambda \left[f(p_1) f(p_2) \frac{\partial}{\partial(p_3 - p_4)_\mu} f(p_3 - q + \lambda q) f(p_4 - \lambda q) - f(p_3) f(p_4) \frac{\partial}{\partial(p_1 - p_2)_\mu} f(p_1 + q - \lambda q) f(p_2 + \lambda q) \right]. \quad (10)$$

This type-II structure contributes in those interaction channels corresponding to isovector states. The Dirac matrices appear in the combinations:

$$G_1(i\gamma_5 \otimes i\gamma_5), \quad G_2(\gamma^\nu \otimes \gamma_\nu + \gamma^\nu \gamma_5 \otimes \gamma_\nu \gamma_5), \quad G_5(1 \otimes 1). \quad (11)$$

Turning to the isovector axial current, the type-I terms are again present. These involve the matrix combinations:

$$G_1 \epsilon^{abc} (\tau^c \otimes i\gamma_5 \tau^b), \quad G_2(\gamma^\nu \gamma_5 \otimes \gamma_\nu \tau^a + \gamma^\nu \otimes \gamma_\nu \gamma_5 \tau^a), \quad G_3(\gamma^\nu \gamma_5 \tau^a \otimes \gamma_\nu), \\ G_4(\gamma^\nu \tau^a \otimes \gamma_\nu \gamma_5), \quad G_5 \epsilon^{abc} (i\gamma_5 \tau^b \otimes \tau^c). \quad (12)$$

There are no type-II pieces in this current, but a third kind of nonlocal structure does occur,

$$\begin{aligned}
J_{(III)}^\mu = & \frac{i}{(2\pi)^{12}} \sum_i G_i \int \prod_n d^4 p_n \bar{\psi}(p_1) \Gamma_i^\alpha \psi(p_3) \bar{\psi}(p_2) \Omega_{i\alpha} \psi(p_4) \delta(p_1 + p_2 + q - p_3 - p_4) \\
& \times \int_0^1 d\lambda \left[f(p_2) f(p_3) \frac{\partial}{\partial(p_1 + p_4)_\mu} f(p_1 + q - \lambda q) f(p_4 - \lambda q) \right. \\
& \left. - f(p_1) f(p_4) \frac{\partial}{\partial(p_2 + p_3)_\mu} f(p_2 + \lambda q) f(p_3 - q + \lambda q) \right]. \quad (13)
\end{aligned}$$

The relevant terms in this case are:

$$G_1(i\gamma_5 \tau^a \otimes 1), \quad G_2 \epsilon^{abc} (\gamma^\nu \gamma_5 \tau^c \otimes \gamma_\nu \tau^b), \quad G_5(i\gamma_5 \otimes \tau^a). \quad (14)$$

It is straightforward to see that dependence on the path, λ , does not appear in the longitudinal components of the currents. Since the form factor depends only on the square of its argument, one has in the case of type-I contributions

$$q_\mu \frac{\partial}{\partial(p_1 + p_3)_\mu} f(p_1 + \lambda q) f(p_3 - q + \lambda q) = \frac{1}{2} \frac{d}{d\lambda} f(p_1 + \lambda q) f(p_3 - q + \lambda q). \quad (15)$$

The λ integral in $q_\mu J_{(I)}^\mu$ is then trivial, and produces a difference in form factors. Similar results can be seen to hold for the longitudinal components of the other nonlocal structures (10,13).

Useful checks on the above expressions for the currents are provided by various Ward identities which follow from (partial) current conservation [30]. In the case of the axial current, an extension of the arguments in Ref. [23] can be used to show that the Gell-Mann–Oakes–Renner (GMOR) relation [31] holds. For the vector currents, we have checked that the two-point correlator of vector currents is purely transverse, that the γqq Ward identity is satisfied, that the pion charge is unity, and that the low-energy theorem for the anomalous decay $\pi^0 \rightarrow \gamma\gamma$ is satisfied.

III. PROPAGATORS AND COUPLINGS TO CURRENTS

A. Quark propagator

The first step in the calculations is to construct the dressed quark propagator, by means of the corresponding Schwinger–Dyson equation (SDE). We treat it in the ladder approximation, which is equivalent to working at leading order in the $1/N_c$ expansion. Fig. 1 gives an illustration of the diagrams that are summed in this approximation. In terms of a momentum-dependent quark “mass” $m(p)$ defined from the dressed quark propagator by

$$S_F^{-1}(p) = \not{p} - m(p), \quad (16)$$

this equation can be written as¹

$$m(p) = m_c + iG_1 f^2(p) \text{Tr} \int \frac{d^4 k}{(2\pi)^4} \frac{\not{k} + m(k)}{k^2 - m^2(k)} f^2(k). \quad (17)$$

The dressing at this order occurs only through the interaction in the isoscalar scalar channel, G_1 . The integral here is very similar to that appearing in the quark condensate, apart from the extra interaction form factors. Just as in the original NJL model, the dynamical generation of quark masses is intimately connected with the appearance of a non-zero condensate. In our numerical treatment of the model we evaluate loop integrals like that in (17) in Euclidean space, since the form factor has been defined for Euclidean momenta. Physical results are then obtained by analytically continuing back to Minkowski space. Notice that the separable nature of the interaction produces a great simplification since the dependence on the external momentum p factorizes out of the loop integral.

The solution to the SDE (17) can be written simply as

$$m(p) = m_c + (m(0) - m_c) f^2(p). \quad (18)$$

Hence to obtain the quark mass it is necessary to determine only the constant $m(0)$. This can be done easily using iterative methods. In practice we choose to use equation (17) to

¹Here ‘Tr’ is used to denote a trace over flavour, colour and Dirac indices; the symbol ‘tr’ will later be used to indicate a trace over Dirac indices only.

determine the parameter G_1 for a given value of $m_0(0)$, the zero-momentum quark mass in the chiral limit.

The denominator of the quark propagator, $p^2 - m^2(p^2)$, does not have a zero at positive (Minkowski) p^2 if $m(0)$ is sufficiently large. This property provides a sufficient, although not strictly a necessary, condition for confinement. There are still poles in the quark propagator, but they are shifted into the complex p^2 plane. Such behaviour is not uncommon in models of quark confinement based on the solution of a Schwinger–Dyson equation [21,22,32,33] in the ladder approximation. Because of the simplifications due to the separable interaction, the present model provides a convenient setting in which to investigate this mechanism for confinement. As pointed out by Lee and Wick [34] (see also [35]), particles which have a complex mass of this type should not appear as asymptotic states if one is to have a unitary S-matrix. When amplitudes have been defined in Euclidean space, the prescription for analytically continuing them back to Minkowski space must respect this requirement, as described in more detail in Subsec. III C.

B. Meson propagators

The meson masses and vertex functions are found using the Bethe–Salpeter equation (BSE). For consistency with the SDE (17), we work in the ladder approximation. At this level, the separable interaction allows the $\bar{q}q$ scattering matrix, T , to be written in the form

$$T(p_1, p_2, p_3, p_4) = \prod_n f(p_n) \delta(p_1 + p_2 - p_3 - p_4) \hat{T}(q), \quad (19)$$

where we have denoted the total momentum of the $\bar{q}q$ pair by $q = p_1 - p_3 = p_4 - p_2$. The BSE, shown schematically in Fig. 2, may be conveniently expressed in terms of \hat{T} as

$$\hat{T}(q) = G + G J(q) \hat{T}(q), \quad (20)$$

where G is simply a matrix of the coupling constants from the action (1–4) and $J(q)$ is composed of the loop integrals

$$J_{ij}(q) = i\text{Tr} \int \frac{d^4 p}{(2\pi)^4} f^2(p_+) f^2(p_-) \Gamma_i S_F(p_-) \Gamma_j S_F(p_+), \quad (21)$$

where we have introduced $p_{\pm} = p \pm \frac{1}{2}q$. The quark propagators to be used in (21) are the dressed propagators obtained by solving the ladder SDE.

The mesonic bound states are located at the poles of \hat{T} . These can be determined from the equation

$$\det(1 - GJ(q)) = 0. \quad (22)$$

The form of the action means that the matrix G is diagonal with respect to flavour and Lorentz structures. The scattering matrix, however, is only block-diagonal, since certain off-diagonal elements of J may be non-zero. In particular there is a loop integral that leads to mixing between the pseudoscalar and longitudinal axial channels. This πa_1 (and $\eta^* f_1$) mixing is an example of the “partial Higgs mechanism” familiar from effective Lagrangians of π, ρ and a_1 mesons [36,37]. It leads to an axial as well as a pseudoscalar vertex function for the pion and η^* . With each flavour having an equal current quark mass, no such mixing occurs between the scalar and vector channels, as can be seen from the fact that the integrand in the corresponding element of (21) is odd under $p \rightarrow -p$. The absence of such a mixing means that the longitudinal vector channel is quite independent of the scalar one. It is therefore important to check that a pole does not develop in the former channel, since that would be unphysical.

For later ease of reference, we label the various elements of J as follows for the Dirac matrices inserted:

$$\begin{aligned} J_{SS} &: 1 \otimes 1, & J_{VV}^T &: T_{\mu\nu}(\gamma^\mu \otimes \gamma^\nu), & J_{VV}^L &: q^{-2}(-i\gamma_5 \otimes i\gamma_5), \\ J_{PP} &: i\gamma_5 \otimes i\gamma_5, & J_{AP} &: m_\pi^{-1}(-i\gamma_5 \otimes i\gamma_5), & J_{PA} &: m_\pi^{-1}(i\gamma_5 \otimes i\gamma_5), \\ J_{AA}^T &: T_{\mu\nu}(\gamma^\mu \gamma_5 \otimes \gamma^\nu \gamma_5), & J_{AA}^L &: m_\pi^{-2}(-i\gamma_5 \otimes i\gamma_5), \end{aligned} \quad (23)$$

where $T_{\mu\nu}$ is the transverse projector,

$$T_{\mu\nu} = g_{\mu\nu} - \frac{q_\mu q_\nu}{q^2}. \quad (24)$$

In this basis, $J_{AP} = J_{PA}$.

Near to the pole corresponding to a particular particle the relevant part of \hat{T} may be represented as

$$\frac{\overline{V}(q) \otimes V(q)}{m^2 - q^2}, \quad (25)$$

where $V(q)$ denotes the appropriate vertex function and any polarization indices have been suppressed. The vertex functions for the final and initial states are related by $\overline{V} = \gamma^0 V^\dagger \gamma^0$. For the particles of interest, they are:

$$\begin{aligned} V_\pi(q) &= (g_{\pi qq} - m_\pi^{-1} \tilde{g}_{\pi qq} \not{q}) i \gamma_5 \tau^a, & V_\sigma(q) &= g_{\sigma qq}, \\ V_{\rho s}(q) &= g_{\rho qq} \not{q}_s \tau^a, & V_{a_1 s}(q) &= g_{a_1 qq} \not{q}_s \gamma_5 \tau^a, & V_{\omega s}(q) &= g_{\omega qq} \not{q}_s, \\ V_{\eta^*}(q) &= (g_{\eta^* qq} - m_{\eta^*}^{-1} \tilde{g}_{\eta^* qq} \not{q}) i \gamma_5, & V_{a_0}(q) &= g_{a_0 qq} \tau^a. \end{aligned} \quad (26)$$

For all particles except the pseudoscalars there is no mixing, and so each has a single coupling constant g_{iqq} describing the coupling of an on-shell meson to quarks. These couplings are related to the corresponding loop integrals (21) by

$$\frac{1}{g_{iqq}^2} = (-1)^S \frac{dJ_{ii}}{dq^2} \bigg|_{q^2=m^2}, \quad (27)$$

where S is the spin of the meson. The couplings of the pion to quarks, $g_{\pi qq}$ and $\tilde{g}_{\pi qq}$, are given by:

$$g_{\pi qq}^2 = -G_1 \frac{\left(1 - G_2 J_{AA}^L(m^2)\right)}{D'_\pi(m^2)}, \quad g_{\pi qq} \tilde{g}_{\pi qq} = \frac{G_1 G_2 J_{PA}(m^2)}{D'_\pi(m^2)}, \quad (28)$$

where the prime indicates a derivative with respect to q^2 and the pseudoscalar-axial determinant $D_\pi(q^2)$ is defined to be:

$$D_\pi(q^2) = \left(1 - G_1 J_{PP}(q^2)\right) \left(1 - G_2 J_{AA}^L(q^2)\right) - G_1 G_2 J_{AP}^2(q^2). \quad (29)$$

Similar expressions hold for the couplings of the η^* , with G_5 and G_4 playing the roles of G_1 and G_2 respectively.

C. Loop integrals

In Euclidean space, the loop integrals in the BSE (21) take the form

$$J_{ij}(q^2) = -N_c N_f \int \frac{d^4 p}{(2\pi)^4} \frac{f^2(p_+) f^2(p_-) t_{ij}(p^2, q^2, p \cdot q)}{(p_+^2 + m_+^2)(p_-^2 + m_-^2)}, \quad (30)$$

where t_{ij} is the appropriate Dirac trace and all momenta are to be understood as Euclidean. We have introduced m_{\pm} here to denote the quark mass evaluated at p_{\pm} . Consider this integral evaluated at some timelike momentum, $q = (\underline{0}, iq_0)$. For a confining parameter set, each quark propagator considered as a function of energy has four poles at complex energies corresponding to a pair of complex-conjugate poles in p^2 . As q_0 is increased these poles are translated parallel to the imaginary p_4 axis. For any given value of $|p|$, there is a value of q_0 for which the poles of the p_- and p_+ quark propagators meet on the real p_4 axis, pinching the contour of integration. For larger values of q_0 the poles cross the axis and may contribute an imaginary part to the propagator in the meson channel, depending on the prescription used to continue the integral beyond the pinch point.

The usual prescription based on Wick rotation of the integration contour would lead to an imaginary part of the meson propagator starting at the minimum value of q_0 for which the contour is pinched. This would correspond to the opening of a threshold for decay of a meson into other states, and as described above (Subsec. III A) is inappropriate here.

One possible continuation, originally suggested by Cutkosky et al. [35], amounts to the deformation of the integration contour displayed in Fig. 3. This prescription ensures that the resulting meson propagator does not develop an imaginary part above the pseudo-threshold where the contour is pinched by the complex poles, although it does mean that the propagator cannot be analytically continued past that point. Such a method is by no means unique but it was shown in Ref. [35] to be consistent with the requirements of unitarity and macrocausality. As discussed by both Cutkosky et al. [35] and Lee and Wick [34], microcausality violations can occur in models with a Euclidean metric and states of complex mass. However, in order to measure such violations, Lee and Wick [34] have estimated that one

would need to create a wave packet of width $\ll \gamma^{-1}$, where the complex mass is $M + \frac{1}{2}i\gamma$. In any event, microcausality in the model is intrinsically broken by the use of an action with nonlocal interactions.

In evaluating these integrals numerically, we take a contour in p_4 that runs along the real axis. For energies q_0 above the pseudo-threshold, the prescription we use means that we have to add in contributions from the residues of the poles that have crossed the axis. Both the naive integral over Euclidean four-momentum in (30) and the residue contributions diverge at the pinch point, although these divergences cancel to leave a finite result [35]. The cancellation occurs at the level of the integrated result rather than at all values of the three-momentum flowing round the loop. In our numerical work, we therefore need to regulate the two contributions when evaluating them separately. We subtract off a function which has the same divergence as the naive integral when p lies within a radius Δ of the pinch point. A similar function is used to cancel the divergent part of the residue contribution when $|p|$ is less than Δ from its pinch value and is chosen to cancel exactly with the piece that has been cut out of the naive integral. We have checked that our results are independent of the value of the regularizing parameter Δ .

It should be noted that the quark propagator of the present model has many complex-conjugate pairs of poles. Such an analytic structure is also found in the pion propagator of the NJL model within the Pauli–Villars regularization scheme [38]. In our model these poles are present for both confining and non-confining parameter sets and their positions depend on the detailed behaviour of the form factor for large momenta. We therefore regard them as unphysical artifacts of the model. For the parameter sets considered here, the next set of poles would result in another pseudo-threshold at energies of ~ 2 GeV. Since the model is not intended to be credible at such momenta, these extra poles do not present a practical problem.

D. Current couplings

The electromagnetic or weak decay constant of a meson is given by the matrix element between the vacuum and that meson of the vector or axial current. In the present model one needs to include contributions from both the usual local current and the nonlocal pieces described in Sec. II. The corresponding diagrams are shown in Fig. 4.

We consider first the pion decay constant. The loop integral arising from the local part of the axial current is very similar to J_{AP} , except that only two (rather than four) form factors are present. One must also include a contribution from the $G_1(i\gamma_5\tau^a \otimes 1)$ term with type-III structure (13) in the axial current. As described in Ref. [23], this piece can be written as a sum of terms each of which factorizes into a loop integral somewhat similar to that in the scalar quark condensate, together with a loop with a pseudoscalar insertion and a pion vertex function. It is convenient to refer to these loops as being one-quark or two-quark, according to the number of quark propagators involved. The contribution of the diagram to f_π is

$$\frac{iG_1}{2m_\pi^2} \int \frac{d^4k}{(2\pi)^4} \frac{\text{Tr}[\not{k} + m(k^2)]}{k^2 - m^2(k^2)} \int \frac{d^4p}{(2\pi)^4} \frac{\text{Tr}V_\pi(q)(\not{p}_- + m_-)\gamma_5\tau^a(\not{p}_+ + m_+)}{(p_+^2 - m_+^2)(p_-^2 - m_-^2)} f(p_+)f(p_-) \\ \times \left[f^2(k) \left(f^2(p_+) + f^2(p_-) \right) - f(p_+)f(p_-)f(k) \left(f(k+q) + f(k-q) \right) \right]. \quad (31)$$

In the extended model there is another nonlocal contribution which is induced by the term $G_2(\gamma^\nu \otimes \gamma_\nu \gamma_5 \tau^a)$ with type-I structure (8) in the axial current. The one-quark loop in this case has a vector insertion. Although the vacuum expectation value of $\bar{\psi}\gamma^\nu\psi$ vanishes by Lorentz invariance, a non-zero integral is produced by a combination of form factors that is anti-symmetric in the loop momentum. The contribution of this diagram to f_π is

$$\frac{-iG_2}{2m_\pi^2} \int \frac{d^4k}{(2\pi)^4} \frac{\text{Tr}\gamma^\nu[\not{k} + m(k^2)]}{k^2 - m^2(k^2)} f(k) \left(f(k+q) - f(k-q) \right) \\ \times \int \frac{d^4p}{(2\pi)^4} \frac{\text{Tr}V_\pi(q)(\not{p}_- + m_-)\gamma_\nu\gamma_5\tau^a(\not{p}_+ + m_+)}{(p_+^2 - m_+^2)(p_-^2 - m_-^2)} f^2(p_+)f^2(p_-). \quad (32)$$

These pieces of f_π arising from the nonlocal current make significant numerical contributions and are needed in order to satisfy the Gell-Mann–Oakes–Renner relation [23,30].

A determination of the coupling strength of the a_1 particle to the transverse axial current requires the evaluation of very similar diagrams to those involved in f_π . However, an important difference from the analogous nonlocal diagrams for f_π arises because the path-dependent integral over λ for the transverse current is non-trivial. In this case a numerical integration over λ is also required. With a type-I nonlocal structure (8), λ is only present in form factors associated with one of the loops. This is not so for contributions induced by type-II (10) or type-III (13) terms in the current, where the integrals for the one- and two-quark loops do not factorize.

The couplings responsible for the electromagnetic decays of the vector mesons can be evaluated in a similar manner. Again the nonlocal contributions are numerically important and are essential if Ward identities such as

$$q^\mu i \int d^4x e^{iqx} \langle 0 | T\{ J_\mu^a(x) \mathcal{O}(0) \} | 0 \rangle = 0 \quad (33)$$

are to be satisfied.

A common scheme to describe electromagnetic couplings in the literature [39–41], sometimes called the impulse approximation, involves the γqq vertex only, neglecting irreducible couplings of the photon to more than two quarks. The γqq vertex itself is chosen to be of the Ball–Chiu [42] form. For the model studied here, use of the impulse approximation is not an appropriate prescription for the calculation of electromagnetic observables. For example, as discussed in Sec. VI, it would not yield the correct value for the pion charge. In this model, the electromagnetic couplings are specified once a particular ansatz has been chosen for the nonlocal part of the vector current. The uncertainty inherent in the construction of the transverse part of the current is discussed in Sec. II. Despite this, gross features of the nonlocal current would remain unchanged with different path ansatze.

The dressed γqq vertex in this model is described in some detail below since it is a necessary ingredient in the calculation of many electromagnetic processes. An important constraint on the structure of this vertex, Γ_μ , is provided by the Ward-Takahashi identity

$$q^\mu \Gamma_\mu(p, q) = S_F^{-1}(p_+) - S_F^{-1}(p_-), \quad (34)$$

where q is the photon momentum flowing away from the vertex and p is the momentum flowing through the vertex. (The isospin structure has been suppressed here.)

The various pieces of the full γqq vertex within this approach are shown diagrammatically in Fig. 5. From the local current, there is simply a contribution to Γ_μ of the usual form, γ_μ . The nonlocal current induces contributions where there is a closed one-quark loop, similar to those in the pion decay constant discussed above. In the electromagnetic case, the diagram where the closed loop has a scalar insertion can be simplified by using the SDE (17) to express it in the form

$$- \left(m(0) - m_c \right) \int_0^1 d\lambda \frac{\partial}{\partial p^\mu} f^2 \left(p + (\lambda - \frac{1}{2})q \right). \quad (35)$$

Added to the local contribution, this would give the full vertex in a version of the model without vector mesons. Now, as a special case of Eq. (15), we have that

$$q^\mu \frac{\partial}{\partial p^\mu} f^2 \left(p + (\lambda - \frac{1}{2})q \right) = \frac{d}{d\lambda} f^2 \left(p + (\lambda - \frac{1}{2})q \right). \quad (36)$$

The λ integral involved in $q^\mu \Gamma_\mu$ is therefore trivial, and so the Ward identity for the γqq vertex (34) can be seen to be satisfied by the sum of γ^μ and (35).

In the extended model with vector-meson degrees of freedom, there is another contribution to Γ_μ involving a one-quark loop with a vector insertion, specifically,

$$- i\gamma_\nu f(p_-) f(p_+) G_2 N_c N_f \int \frac{d^4 k}{(2\pi)^4} \frac{4k^\nu}{k^2 - m^2(k^2)} \int_0^1 d\lambda \frac{\partial}{\partial k^\mu} f(k - q + \lambda q) f(k + \lambda q). \quad (37)$$

In addition there are pieces which contain the propagator of an intermediate $\bar{q}q$ state, as constructed from the ladder BSE (20), in the vector channels. The contribution of the longitudinal channel to Γ_μ is

$$i \frac{\not{q}}{q^2} f(p_-) f(p_+) \frac{G_2 N_c N_f}{1 - G_2 J_{VV}^L(q)} \int \frac{d^4 k}{(2\pi)^4} \frac{f(k_-) f(k_+)}{(k_-^2 - m_-^2)(k_+^2 - m_+^2)} \times \text{tr} \tilde{\Gamma}_\mu(k, q) (\not{k}_- + m_-) \not{q} (\not{k}_+ + m_+), \quad (38)$$

while the transverse channel gives

$$i \left(\gamma^\nu - \frac{q^\nu \not{q}}{q^2} \right) f(p_-) f(p_+) \frac{G_2 N_c N_f}{1 - G_2 J_{VV}^T(q)} \int \frac{d^4 k}{(2\pi)^4} \frac{f(k_-) f(k_+)}{(k_-^2 - m_-^2)(k_+^2 - m_+^2)} \times \text{tr} \tilde{\Gamma}_\mu(k, q) (\not{k}_- + m_-) \gamma_\nu (\not{k}_+ + m_+), \quad (39)$$

where $\tilde{\Gamma}^\mu(k, q)$ is the two-quark-irreducible γqq vertex consisting of the sum of γ^μ , (35) and (37). In these expressions, m_\pm denotes the quark mass evaluated at k_\pm .

To check that the additional contributions (37-39) in the extended model are consistent with the Ward identity (34), we note first that the quark propagator is unchanged and so the sum of the local piece and (35) still saturates the identity. In the contribution of expression (37) to $q^\mu\Gamma_\mu$, Eq. (15) enables the integration over the path variable to be performed. This part of $q^\mu\Gamma_\mu$ is then

$$-i\frac{\not{q}}{q^2}f(p_-)f(p_+)G_2N_cN_f\int\frac{d^4k}{(2\pi)^4}\frac{4q\cdot k}{k^2-m^2(k^2)}f(k)\left(f(k+q)-f(k-q)\right). \quad (40)$$

The purely transverse piece (39), which involves a propagating ρ -meson, obviously does not contribute to the Ward identity. Thus cancellation must occur between (40) and the piece coming from (38). To demonstrate this explicitly, we make use of the fact that $q^\mu\tilde{\Gamma}_\mu$ is given by the sum of (40) and the right-hand-side of (34). The contribution to $q^\mu\Gamma_\mu$ involving the longitudinal $\bar{q}q$ intermediate state (38) can then be expressed as

$$i\frac{\not{q}}{q^2}\frac{G_2N_cN_f}{1-G_2J_{VV}^L(q)}f(p_-)f(p_+)\left[\int\frac{d^4k}{(2\pi)^4}\frac{\text{tr}(\not{q}+m_-+m_+)(\not{k}_-+m_-)\not{q}(\not{k}_++m_+)}{(k_+^2-m_+^2)(k_-^2-m_-^2)}f(k_+)f(k_-) - G_2J_{VV}^L(q)\int\frac{d^4k}{(2\pi)^4}\frac{4q\cdot k}{k^2-m^2(k^2)}f(k)\left(f(k+q)-f(k-q)\right)\right]. \quad (41)$$

The Dirac trace in the first line of the above expression may be written as

$$4(q\cdot k_-)(k_+^2-m_+^2)-4(q\cdot k_+)(k_-^2-m_-^2). \quad (42)$$

Hence in each of the resulting terms, one of the factors $k_\pm^2-m_\pm^2$ can be cancelled in the denominator of the integral. Shifting the integration variable from k to k_\pm as appropriate, the first term inside the square brackets of (41) may be rewritten in the same form as the second, demonstrating the required cancellation. Note that the discussion above has referred to the presence of the G_2 coupling in the isovector interaction channel. The results in the isoscalar channel are completely analogous, with the replacement of G_2 by G_3 .

For the purpose of practical calculations, it is convenient to collect together the various contributions to the vertex in the form

$$\begin{aligned}\Gamma_\mu(p, q) = & \gamma_\mu Q + \left(\gamma_\mu - \frac{q_\mu q}{q^2} \right) f(p_-) f(p_+) B(q^2) \\ & - 2Q \int_0^1 d\lambda (p + (\lambda - \frac{1}{2})q)_\mu m'(p + (\lambda - \frac{1}{2})q),\end{aligned}\quad (43)$$

where the prime denotes a derivative with respect to the square of the momentum argument and we have reinstated the flavour structure using the charge matrix $Q = \frac{1}{2}(\tau^3 + \frac{1}{3})$. The function $B(q^2)$ accounts for the presence of vector mesons in the model and has the form $B(q^2) = \frac{1}{2}(\tau^3 B_2(q^2) + \frac{1}{3}B_3(q^2))$ where the functions $B_i(q^2)$ are

$$\begin{aligned}B_i(q^2) = & \left\{ \frac{1}{1 - G_i J_{VV}^T(q)} \right\} \left\{ A_i(q) + iG_i N_c N_f \int \frac{d^4 k}{(2\pi)^4} \frac{f(k_-) f(k_+)}{(k_-^2 - m_-^2)(k_+^2 - m_+^2)} \right. \\ & \times \left[\left(4m_- m_+ - 4k^2 + q^2 + \frac{8}{3} \left(k^2 - \frac{(q \cdot k)^2}{q^2} \right) \right) \right. \\ & \left. \left. - \frac{8}{3} (m_+ + m_-) \left(k^2 - \frac{(q \cdot k)^2}{q^2} \right) \int_0^1 d\lambda m' \left(k + (\lambda - \frac{1}{2})q \right) \right] \right\},\end{aligned}\quad (44)$$

and the $A_i(q^2)$ in the above equation originate from the one-quark loop with a vector insertion and are given by

$$\begin{aligned}A_i(q^2) = & -\frac{8i}{3} G_i N_c N_f \int \frac{d^4 k}{(2\pi)^4} \frac{k^2 - (q \cdot k)^2/q^2}{k^2 - m^2(k^2)} \\ & \times \int_0^1 d\lambda \left(f'(k + \lambda q) f(k - q + \lambda q) + f(k + \lambda q) f'(k - q + \lambda q) \right).\end{aligned}\quad (45)$$

Writing $A_i(q^2)$ and $B_i(q^2)$ in Euclidean-space form and performing an integration by parts on (45), one finds that $B_i(0) = 0$. This is simply a consequence of the differential form of (34),

$$\Gamma_\mu(p, 0) = Q \frac{\partial}{\partial p^\mu} S_F^{-1}(p).\quad (46)$$

Hence, in evaluating processes where the photon is on-shell, the γqq vertex is unchanged by the existence of vector-meson degrees of freedom in the model.

For the coupling of an on-shell vector meson to the vector current, one evaluates a quark loop between the meson vertex function and that part of the γqq vertex which does not include the contribution from the propagating transverse vector channel, (39). Attempting to include such a diagram would merely amount to the addition of another bubble onto the

vector-meson chain. Since (39) is purely transverse, the Ward identity for the vertex still holds.

IV. NUMERICAL FITS

The model as defined in Sec. II above has seven parameters: the current quark mass (m_c), the range of the form factor (Λ) and five possible coupling constants. Considering first the couplings G_1 and G_2 only, we have chosen to fit the quantities: $m_\pi = 140$ MeV, $f_\pi = 93$ MeV and $m_\rho = 770$ MeV, which do not depend on the remaining three couplings. This leaves one parameter undetermined which we have taken to be $m_0(0)$, the zero-momentum quark mass obtained in the chiral limit of the SDE (17). Each of the other three couplings may then be independently fixed to reproduce the mass of the corresponding meson: G_3 is set by requiring $m_\omega = 783$ MeV ; G_4 by $m_{f_1} = 1282$ MeV and G_5 by $m_{a_0} = 982$ MeV. The meson masses are determined from Eq. (22), whilst f_π is given by the coupling of the pion to the axial current. The contributions to f_π from the nonlocal pieces of the current are significant: the scalar and vector loop terms described in the previous section are respectively $\sim 35\%$ and $\sim -10\%$ of the total value.

In terms of $m_0(0)$, the possible fits have a restricted range. Having a coupling strong enough to realize confinement requires that $m_0(0) \gtrsim 270$ MeV. Below that value, the model should only be used up to an energy corresponding to the appearance of the $\bar{q}q$ continuum at twice the value of the (purely real) quark mass. In fact only a very limited range of non-confining sets are possible because the empirical masses of the vector mesons are located in this continuum for $m_0(0) \lesssim 250$ MeV.

An upper limit on the acceptable values for $m_0(0)$ is imposed by the behaviour of the meson propagators above the pseudo-threshold. The dramatic changes of behaviour which can occur beyond this point may be seen in Fig. 6, where the denominators of the propagators in various scattering channels are plotted for a parameter set with $m_0(0) = 300$ MeV. In this case the pseudo-threshold occurs at an energy of 895 MeV. For larger values of $m_0(0)$

this energy decreases. As suggested by the behaviour in Fig. 6, for large enough $m_0(0)$ two additional poles appear in the transverse-vector channel above the ρ pole. The first of these extra poles has a residue of the wrong sign to describe a physical particle. Although one might hope to consider parameter sets with the extra poles, provided that they lie well above the energies of interest, in practice this is possible only for values of $m_0(0)$ within a very narrow range, $\sim 320 - 330$ MeV.

A pronounced change in behaviour beyond the pseudo-threshold also occurs in the longitudinal-vector channel and seems to be important in ensuring that no poles are present in this channel. An unphysical pole does occur, however, in the pion propagator (Fig. 6). This unwanted pole is located between 1.3 and 1.45 GeV, depending on the parameter set used. One should therefore only attempt to use the model at smaller energies. Although a similar pole also appears in the η^* propagator, it lies at a higher energy than in the pion case.

We present here numerical results for parameter sets which lie near each edge of the acceptable range for $m_0(0)$. The variation of results over the full range is generally monotonic; where it is not, the dependence on $m_0(0)$ is fairly weak. Specifically, we have chosen to work with $m_0(0) = 280$ MeV (henceforth referred to as set A) and 320 MeV (set B). Details of these parameter sets are given in Table 1. Values of the zero-momentum quark masses calculated for these parameters at non-zero m_c are also quoted in Table 1. A simple estimate of the importance of higher-order terms in the chiral expansion is provided by the following ratio, which would equal unity if the GMOR relation were exact,

$$r = -m_c \frac{\langle \bar{\psi} \psi \rangle_0}{m_\pi^2 f_\pi^2}, \quad (47)$$

where the quark condensate is evaluated in the chiral limit. The values of r for the parameter sets in Table 1 indicate that terms of order m_c^2 and higher contribute at the $\sim 10\%$ level.

In the chiral limit, the model quark condensate is $-(206\text{MeV})^3$ and $-(189\text{MeV})^3$ for sets A and B respectively. With non-zero current-quark mass, the condensate integral is quadratically divergent. If it is regulated by subtracting the perturbative condensate, slightly

higher values of $-(212\text{MeV})^3$ and $-(193\text{MeV})^3$ are obtained. These are similar in size to values for the condensate determined from QCD sum rules [43,44]. However one should bear in mind the fact that the condensate in QCD is a renormalized and scale-dependent quantity and so one ought to be careful about comparing it directly with the value obtained in a model of this type.

Table 2 lists the positions of the first few sets of poles in the quark propagator. Since we only consider the first group of poles to have physical relevance, the model should be used only for energies of less than twice the real part of the second set of poles. This limit is 2.3 GeV and 1.8 GeV for the parameter sets A and B, and so is sufficiently far above the upper limit imposed by the unphysical pole in the pion channel not to be of practical concern.

In Table 3, the calculated meson masses are given, along with their on-shell couplings to quarks, as defined in Eqs. (27–29). The scalar isoscalar state is rather light. For comparison, the mass of the corresponding particle in the NJL model [2,3,26] is $m_\sigma^2 = m_\pi^2 + 4m^2$, where m is the mass of the constituent quark. Interestingly, the σ mass in our model varies only slowly with the dynamical quark mass. Although rather low, the σ masses obtained in the model lie within the range of values for the mass of the scalar isoscalar meson determined from a number of analyses of low-energy $\pi\pi$ scattering [45].

The calculated a_1 mass is somewhat smaller than the observed 1260 MeV [46]. In the case of parameter set A, it lies a little below the pseudo-threshold, but for most of the range of admissible $m_0(0)$ it is above that energy. The $\rho - a_1$ mass splitting increases with increasing constituent quark mass, although not so rapidly as suggested by the NJL [26] expression, $m_{a_1}^2 = m_\rho^2 + 6m^2$, obtained from the derivative expansion of the bosonized model. As a consequence of the upper bound on the constituent mass, which follows from the effect of the pseudo-threshold on the transverse-vector channel, it is not possible to simultaneously reproduce the empirical values for both the ρ and a_1 masses in the ladder approximation.

Since there are important flavour-mixing effects in the isoscalar pseudoscalar sector, a realistic calculation for these mesons would require a three-flavour version of the model. The η^* mass in the present two-flavour model should not therefore be directly compared

with experiment. It is nevertheless reassuring that this mass lies between the physical η and η' masses of 547 and 958 MeV respectively. Another possibly important feature in the description of the state is the axial-pseudoscalar mixing with the longitudinal f_1 channel. Indeed, in a Bethe-Salpeter study of a three-flavour model [47], the $\not{q}\gamma_5$ term in the vertex function was found to make significant contributions to the mass (~ 70 MeV) and decay constant of the η . A similar effect has also been found in the NJL model [27]. In the present model, if the f_1 is omitted by setting G_4 to zero, then the η^* mass for parameter set A is reduced by around 20 MeV, whereas for set B it falls by over 110 MeV. These rather different behaviours are another consequence of the dramatic changes in the meson propagators which can occur at the pseudo-threshold. When $G_4 = 0$, the η^* mass lies below the pseudo-threshold for the full range of parameter sets. For non-zero G_4 , the mixing increases the η^* mass and for parameter sets with $m_0(0) \gtrsim 310$ MeV the mass is pushed above the pseudo-threshold, where the effect can be greatly enhanced. In addition, for these parameter sets the gradient of the determinant D_{η^*} (cf. Eq. (29)) changes significantly above the pseudo-threshold and so the coupling of the η^* to quarks is considerably stronger.

V. HADRONIC DECAYS

At leading order in $1/N_c$, the three-meson vertices are calculated from a quark loop with insertions of three vertex functions. We have obtained several physical decay amplitudes from such diagrams with all of the mesons on-shell, where the vertex functions are unambiguous.

For an initial state of momentum q decaying to particles with momenta q_1 and q_2 , the quark propagators in the triangular loop are evaluated at $p \pm \frac{1}{2}q$ and $p + \frac{1}{2}(q_1 - q_2)$. If the initial state has a mass which is greater than twice the real part of the quark pole, then its decay modes will be sensitive to pseudo-threshold effects. By analogy with the loop integral in the BSE for that particle, residue contributions must be taken into account in the three-point diagrams. It is also possible that further residue contributions may be required

if a final-state particle lies above the pseudo-threshold energy, but such a situation does not occur in practice for any of the amplitudes considered.

The couplings that we have considered are defined below, and their numerical values are given in Table 4, along with the corresponding decay widths.

$$\begin{aligned}
\langle \pi^a(q_1) \pi^b(q_2) | \sigma(q) \rangle &= -g_{\sigma\pi\pi} \delta^{ab} \\
\langle \pi^b(q_1) \pi^c(q_2) | \rho^a(q) \rangle &= ig_{\rho\pi\pi} \epsilon^{abc} (q_2 \cdot \epsilon - q_1 \cdot \epsilon) \\
\langle \sigma(q_1) \pi^b(q_2) | a_1^a(q) \rangle &= \frac{1}{2} ig_{a_1\sigma\pi} \delta^{ab} (q_1 \cdot \epsilon - q_2 \cdot \epsilon) \\
\langle \rho^b(q_1) \pi^c(q_2) | a_1^a(q) \rangle &= \epsilon^{abc} (g_{a_1\rho\pi} (\epsilon_\rho^* \cdot \epsilon_{a_1}) - h_{a_1\rho\pi} (q_2 \cdot \epsilon_\rho^*) (q_2 \cdot \epsilon_{a_1})) \tag{48}
\end{aligned}$$

If the sigma meson of the model is to be interpreted as corresponding to the scalar particle of the linear sigma model then its coupling to two pions should be strong. Whilst the values in Table 4 do not indicate a particularly broad state, this width is significantly reduced by the small available phase space. To provide a useful comparison, we consider the prediction for the two-pion coupling $g_{\sigma\pi\pi}$ from the linear sigma model. In that model, the coupling is $g_{\sigma\pi\pi} = (m_\sigma^2 - m_\pi^2)/f_\pi$ which, for the σ masses of parameter sets A and B gives $g_{\sigma\pi\pi} = 1901$ MeV and 2122 MeV respectively. These values are $\sim 30\%$ larger than the results for our model, indicating that the coupling to pions of the scalar meson in the nonlocal NJL model is qualitatively similar to that of the linear-sigma-model particle.

The ρ meson decay width compares reasonably well with the empirical value of 151 MeV. In contrast, the corresponding leading-order calculation in an extended NJL model, using the physical ρ mass, significantly underestimates the decay rate [48]. We find that it is not possible to simultaneously reproduce the empirical mass and decay width of the ρ at leading order in our model. However, if the model parameters for a given $m_0(0)$ are refitted to the ρ width rather than to its mass, the results for observables are not qualitatively different from those of the original fit. For instance, this procedure would increase the ρ mass itself by ~ 20 to 60 MeV.

The coupling $g_{a_1\sigma\pi}$ is not a direct observable, although the process it describes would be involved in the physical decay of $a_1 \rightarrow 3\pi$. The Particle Data Group [46] quotes an

experimental upper bound on the final state $\pi(\pi\pi)_S$ of $\sim 0.7\%$ of the total a_1 width of ~ 400 MeV. The strong couplings obtained here suggest that the model may not be consistent with such a result. However, the situation is far from clear. There is also an amplitude for this final state originating from a direct, four-point $a_1 \rightarrow 3\pi$ diagram which we have not yet calculated. It is conceivable that this might conspire to cancel some of the amplitude for $a_1 \rightarrow \sigma\pi \rightarrow 3\pi$. Furthermore, the two-stage process would have to be integrated over various momenta of the scalar resonance, where the $a_1\sigma\pi$ and $\sigma\pi\pi$ couplings may be reduced from their on-shell values. A hint that this may indeed be the case is provided by the $\sigma\pi\pi$ loop integral, which vanishes at a scalar momentum of around 800 MeV.

The dominant decay mode of the a_1 is to $\rho\pi$. Although the parameter set B does give a credible, broad width, with set A the state seems to be very narrow. Since the final state has a combined mass of 910 MeV, the allowed phase space for the decay is drastically reduced at the model a_1 masses as compared to the empirical mass. Using parameter set A, the a_1 mass is only 946.8 MeV and so the small decay width of 44 MeV may simply be a consequence of the phase-space suppression.

In order to examine whether the $a_1\rho\pi$ coupling is reasonably well described by the model, we compare it with the description of the same process using a phenomenological mesonic Lagrangian. The CCWZ formalism originally developed in Ref. [49] is particularly convenient for this purpose since the a_1 mass can be set to any desired value without violating the constraints of chiral symmetry. A suitable Lagrangian for the comparison is one obtained by converting the simplest Lagrangian in the massive Yang–Mills scheme [36] into its CCWZ equivalent and then adjusting the a_1 mass.² Details of the relevant change of variables can be found in Ref. [37]: the appropriate Lagrangian is equation (5.6) of that paper. We take $f_\pi = 93$ MeV, $m_\rho = 770$ MeV and $Z^2 = 1/2$ as the parameters specifying the original

²A similar conclusion is reached if one starts with the simplest Lagrangian for π , ρ and a_1 in the hidden-symmetry formalism.

massive Yang–Mills Lagrangian. For the empirical a_1 mass of 1230 MeV, this gives a broad state of width 490 MeV. When we use the a_1 masses found in the model with parameter sets A and B, the effective Lagrangian gives significantly smaller widths, 23 and 132 MeV respectively. This suggests that the small widths found in the model are largely due to the the small a_1 mass rather than any underestimate of the coupling strength.

The amplitude for the decay $a_1 \rightarrow \rho\pi$ is a mixture of s and d -wave components. In terms of the decay parameters defined in (48), the ratio of d to s -wave amplitudes is

$$R = -\sqrt{2} \frac{(E_\rho - m_\rho) g_{a_1\rho\pi} + |\mathbf{q}_\rho|^2 m_{a_1} h_{a_1\rho\pi}}{(E_\rho + 2m_\rho) g_{a_1\rho\pi} + |\mathbf{q}_\rho|^2 m_{a_1} h_{a_1\rho\pi}}, \quad (49)$$

where E_ρ and \mathbf{q}_ρ are the energy and three-momentum of the ρ , in the a_1 rest frame. This quantity has been determined by the ARGUS collaboration [50] from τ -decay data to be -0.11 ± 0.02 . The effective Lagrangian approach discussed above requires higher-order couplings in order to obtain a non-zero $h_{a_1\rho\pi}$ and so this ratio provides a test of such higher-order effects. From the values for R in Table 4, we see that, for the parameter set A, the ratio is rather low, but the value for set B is consistent with the observed one. Overall, set B provides the better description of both the a_1 mass and its hadronic decays.

VI. ELECTROMAGNETIC PROCESSES

Further tests of models where mesons are constructed as $\bar{q}q$ composites are provided by electromagnetic processes and form factors that probe the internal meson structure. For this it is necessary to specify the photon-quark coupling, which requires additional assumptions about the form of the nonlocal current, as discussed in Sec. II. The resultant coupling in the present model and the means of calculating the electromagnetic decays of the vector mesons were discussed in Subsec. III D. These photon-vector-meson couplings are defined by

$$\begin{aligned} \langle 0 | J^{\mu a} | \rho_s^b \rangle &= -g_{\rho\gamma} \delta^{ab} \epsilon_s^\mu, \\ \langle 0 | J^\mu | \omega_s \rangle &= -g_{\omega\gamma} \epsilon_s^\mu. \end{aligned} \quad (50)$$

The empirical values, obtained from $\rho \rightarrow e^+e^-$ and $\omega \rightarrow e^+e^-$ [46], are $g_{\rho\gamma} = 0.1177 \text{ GeV}^2$ and $g_{\omega\gamma} = 0.0359 \text{ GeV}^2$. The calculated values for these couplings, given in Table 5, are in reasonable agreement with the experimental ones.

Values for the dimensionless quantities $g_V = \frac{m_V^2}{g_{V\gamma}}$ are also given in Table 5 and may be compared with the results for $g_{\rho\pi\pi}$ in Table 4. Universal coupling of the ρ would predict that $g_\rho = g_{\rho\pi\pi}$ (see, for example, [36,37]). This is clearly violated in the model, although notably less so with parameter set A, where both of these couplings are closer to the empirical ones.

It is interesting to compare the $\rho\gamma$ coupling with the corresponding coupling of the a_1 to the transverse axial current. A coupling strength g_{a_1} can be defined analogously to $g_{V\gamma}$,

$$\langle 0 | J_5^{\mu a} | a_{1s}^b \rangle = -g_{a_1} \delta^{ab} \epsilon_s^\mu. \quad (51)$$

Evaluating this as described in Subsec. III D, we obtain values for g_{a_1} of 0.072 GeV^2 and 0.138 GeV^2 with parameter sets A and B, respectively. No direct experimental measurement of g_{a_1} exists with which to make a comparison, but the quantity does appear in Weinberg's sum rules [51]. If one assumes complete vector and axial-vector meson dominance in Weinberg's first and second sum rules, then one gets the relations

$$\frac{g_{\rho\gamma}^2}{m_\rho^2} - \frac{g_{a_1}^2}{m_{a_1}^2} = f_\pi^2, \quad (52)$$

$$g_{\rho\gamma} = g_{a_1}. \quad (53)$$

The results of the model for parameter set A are consistent with these vector-dominance versions of these sum rules, at the $\sim 15\%$ level. In contrast the results for set B clearly fail to satisfy these relations.

The pion form factor provides a further test of vector-meson dominance (VMD). This quantity receives contributions from the two kinds of diagram shown in Fig. 7. The first of these involves a triangular loop, and is often the only one considered in calculations of the form factor. For a timelike momentum q carried by the external current, the situation is similar to that discussed in Sec. V for the triangle diagrams in hadronic decays, with pseudo-threshold effects appearing at energies beyond twice the real part of the quark pole.

The other kind of diagram in Fig. 7, which we shall refer to as a two-body diagram, is produced by the terms $G_1(i\gamma_5 \otimes i\gamma_5)$ and $G_2(\gamma^\nu\gamma_5 \otimes \gamma_\nu\gamma_5)$ with type-II structure (10) in the nonlocal isovector current. The quark propagators involved are evaluated at $p \pm \frac{1}{2}q_\pi$, and so pseudo-threshold effects are not present. The contribution of these diagrams can be written as a sum over terms, each of which is the product of two loop integrals which are somewhat similar to those in J_{PP} , J_{AP} or J_{AA}^L . Since the path variable appears in form factors associated with both of the loops, the two loops are coupled together. The need for similar two-body contributions has also been noted in the context of models where the four-quark interaction is dependent only on the relative momentum of the $\bar{q}q$ pair [15]. In a model of that type the analogue of the two-body diagram can be reduced to a single two-quark loop, where one of the the πqq vertex functions is modified by the photon. Such diagrams make no contribution to the pion charge, unlike the two-body diagrams in the present model.

The absolute value of the form factor is displayed in Fig. 8, for a parameter set with $m_0(0) = 300$ MeV. Below the ρ meson pole, very little variation with $m_0(0)$ is observed in the results when other parameter sets are used. Also shown on the figure are experimental data points, obtained from Refs. [52,53] for the region of spacelike q^2 and Ref. [54] for timelike q^2 . Below the ρ pole, the model curve is in rather good agreement with the data, although its rise is a little shallower. This is confirmed by the mean-square pion radius, given in Table 5. The values are somewhat smaller than the experimental one [52] of 0.439 ± 0.008 (fm) 2 .

The dashed curve in Fig. 8, labelled VMD, is plotted to test to what extent the model is consistent with the concept of vector meson dominance. Under the assumption of VMD in the photon-pion coupling, the form factor is

$$F_\pi(q^2) = 1 - \frac{g_{\rho\pi\pi}}{g_\rho} \frac{q^2}{q^2 - m_\rho^2}. \quad (54)$$

The ratio of $g_{\rho\pi\pi}$ to g_ρ is underestimated by the model, and as a result the VMD form factor rises somewhat more slowly than the data. Nonetheless the VMD approximation to the model curve is not a bad one, particularly at low q^2 .

An important check on our calculations, both analytic and numerical, is that the pion charge should be unity, $F_\pi(0) = 1$. This result has been verified analytically in the chiral limit [30]. It is also satisfied by our numerical results, to the accuracy of our integration routines. About a third of the pion charge comes from the two-body diagram in Fig. 7, demonstrating the importance of including this contribution.

The individual contributions to the form factor, below the ρ pole, are shown in Fig. 9. The curve labelled “bare” is the contribution from the triangle diagram with the local γqq coupling (the first diagram in the representation of the dressed γqq vertex shown in Fig. 5). The curve labelled “scalar” comes from the triangle diagram with a nonlocal coupling (as in the second diagram of Fig. 5) and a loop with a scalar insertion, given in Eq. (35). This contribution is negligible over the range of q^2 considered. All other contributions are included in the curve labelled “vector”, corresponding to the part of Eq. (43) that is proportional to $B(q^2)$. Since the transverse ρ -meson propagator is contained in the function $B_2(q^2)$ (44), this contribution is the dominant one close to the ρ pole. The contribution of the two-body diagram is relatively small in the vicinity of the ρ . However it varies only slowly with momentum, and so it quite rapidly becomes important at large spacelike momenta. This is as expected since, for large momentum transfer to the pion, the pion vertex functions cut down the triangle-diagram contributions.

It is interesting to note that, away from the pole, much of the variation with momentum is controlled by the “bare” piece of the form factor, which contributes $\sim 77\%$ of the mean-square charge radius $\langle r_\pi^2 \rangle$. Although this term has no ρ pole, when added to the “vector” contribution, the result is close to that of the VMD approximation to the model. This implies cancellation between the “bare” contribution and that of other states above the ρ in the “vector” piece, to leave the ρ pole as the dominant contribution. In contrast, although a similar mean-square radius has been obtained in an extended NJL model [55], most of that value was accounted for by a diagram with an intermediate ρ meson, the bare photon vertex yielding just 32%.

Above the ρ pole, the measured form factor is not well described by the model curve.

A possible explanation is suggested by Fig. 10, which breaks the form factor down into its various contributions for $q^2 > m_\rho^2$. There is a substantial cancellation between the “bare” and “vector” contributions and so the result is likely to be very sensitive to fine details of the model in this regime. This is borne out by the strong dependence of the results in this region on the parameter set chosen. It is also responsible for the prominence of the rather strange structure just above the pseudo-threshold in Fig. 8. This cancellation between large amplitudes suggests that the results of the model should not be regarded as reliable in this region.

The use of the conserved current constructed in Sec. II implicitly ensures that the electromagnetic Ward identities are satisfied by the model. Several examples of these have been already discussed above. Another important one is the amplitude for the decay $\pi^0 \rightarrow \gamma\gamma$, which is an example of an anomalous process. Such processes require a complete set of quark states and so present a problem for the usual NJL model, where the use of a regulator means that high-energy quark states are discarded. In the model studied here, the low-energy theorem for $\pi^0 \rightarrow \gamma\gamma$ is automatically satisfied provided that one includes both of the diagrams shown in Fig. 11. As well as the usual triangle diagram, there is a two-body diagram involving a dressed γqq vertex (43) for one of the photons and a $\gamma qqqq$ vertex for the other. Details of the calculation are given in the Appendix.

The finite current quark masses mean that the physical amplitude differs slightly from its value in the chiral limit. Numerical results for $g_{\pi\gamma\gamma}$, defined from

$$\langle \gamma(q_1)\gamma(q_2)|\pi^0\rangle = \frac{-2\alpha_{EM}}{\pi f_\pi} g_{\pi\gamma\gamma} \epsilon_{\alpha\beta\mu\nu} q_1^\alpha q_2^\beta \epsilon_1^{*\mu} \epsilon_2^{*\nu} \quad (55)$$

are given in Table 5. The deviations from $\frac{1}{2}$, the result in the chiral limit, are small and are consistent with those in the experimental value, $g_{\pi\gamma\gamma} = 0.503 \pm 0.018$ [46].

The related process where one of the photons is off-shell, $\gamma\gamma^* \rightarrow \pi^0$, provides a probe of the structure of the neutral pion. A corresponding form factor may be defined as

$$F_{\pi\gamma}(q^2) = \frac{\langle \gamma^*(q^2)\gamma|\pi^0\rangle}{\langle \gamma(q^2=0)\gamma|\pi^0\rangle}. \quad (56)$$

The CELLO collaboration [56] have quoted five data points for this form factor in the spacelike region, which extends from $-m_\pi^2$. These are shown in Fig. 12, along with the results of the model for a parameter set with $m_0(0) = 300$ MeV. The model results are not sensitive to the choice of parameter set and are dominated by the contribution from the triangle diagram with local photon couplings. They are consistent with the limited data available and comparable to the results obtained in other Bethe–Salpeter approaches [40,41]. There are hopes that improved experimental data will become available, since there are plans to measure the form factor with high precision at Jefferson Lab [57]. Also displayed on Fig. 12 is the VMD prediction for the form factor, given by

$$F_{\pi\gamma}(q^2) = 1 - \frac{2\pi^2 f_\pi}{g_{\pi\gamma\gamma}} \sum_{V=\rho,\omega} \frac{g_{V\pi\gamma}}{g_V} \frac{q^2}{q^2 - m_V^2}, \quad (57)$$

using the model values for the couplings. (The couplings $g_{V\pi\gamma}$, describing the decays $V \rightarrow \pi\gamma$, will be discussed shortly.) In this case, the VMD approximation to the model result is a little poorer than it was for the pion form factor.

Finally, we consider decays of spin-1 mesons into $\pi\gamma$ final states. Schematically, the calculation involves triangle and two-body diagrams, analogous to those of Fig. 11. Just as in the anomalous pion decay the piece of the nonlocal current which gives rise to the two-body diagrams for $V \rightarrow \pi\gamma$ is the type-I term (8) with Dirac structure $G_2(\gamma^\nu\gamma_5 \otimes \gamma_\nu\gamma_5)$. These two-body diagrams do not prove to be numerically important in these decays, producing less than 1% of the total amplitudes. The results for these couplings, as defined by

$$\begin{aligned} \langle \gamma(q_1)\pi^0(q_2)|\omega \rangle &= ieg_{\omega\pi\gamma}\epsilon_{\alpha\beta\mu\nu}q_1^\alpha q_2^\beta \epsilon_\gamma^{*\mu} \epsilon_\omega^\nu, \\ \langle \gamma(q_1)\pi^b(q_2)|\rho^a \rangle &= i\delta^{ab}eg_{\rho\pi\gamma}\epsilon_{\alpha\beta\mu\nu}q_1^\alpha q_2^\beta \epsilon_\gamma^{*\mu} \epsilon_\rho^\nu, \end{aligned} \quad (58)$$

are given in Table 5, along with the corresponding decay widths. In the isospin symmetric case, there is no ϵ^{ab3} component to the $\rho\pi\gamma$ matrix element, so that the decay widths for the charged and neutral ρ mesons are equal. The model results agree well with the experimental values [46],

$$\Gamma(\omega \rightarrow \pi\gamma) = 717 \pm 43 \text{ keV},$$

$$\begin{aligned}\Gamma(\rho^0 \rightarrow \pi^0 \gamma) &= 121 \pm 31 \text{keV}, \\ \Gamma(\rho^\pm \rightarrow \pi^\pm \gamma) &= 68 \pm 8 \text{keV},\end{aligned}\tag{59}$$

the difference between the measured charged and neutral ρ -decays not being considered statistically significant in view of the large error bars [58].

Extending the $\omega\pi\gamma$ amplitude to off-shell photon momenta, we compare our model results to the form factor as measured in Ref. [59]. The reaction $\pi^- p \rightarrow n\omega \rightarrow n\pi^0 \mu^+ \mu^-$ was used to probe the form factor in the range from $4m_\mu^2$ to $(m_\omega - m_\pi)^2$. Using a definition of

$$F_{\omega\pi}(q^2) = \frac{\langle \gamma^*(q^2) \pi | \omega \rangle}{\langle \gamma(q^2 = 0) \pi | \omega \rangle},\tag{60}$$

the model results and experimental data are shown in Fig. 13. A parameter set where $m_0(0) = 300$ MeV has again been used in plotting the model results, which are not sensitive to the set chosen. In common with other theoretical calculations [60] the model is in agreement with the data points at low q^2 but there is a discrepancy with the higher-energy values. It may be that there is some effect on this form factor due to the tail of the ρ' resonance [61]. Also, a potentially important missing ingredient in our calculation is $\omega\phi$ mixing, since a calculation of this form factor within an SU(3) effective Lagrangian approach [62] has found a significant dependence on the mixing strength. Improved data would be needed to draw any firmer conclusions and there are hopes that the experimental situation will be indeed be clarified by forthcoming experiments at VEPP-2M or DAΦNE [58].

In this case, the comparison with the VMD prediction,

$$F_{\omega\pi}(q^2) = 1 - \frac{g_{\omega\rho\pi}}{g_{\omega\pi\gamma} g_\rho} \frac{q^2}{q^2 - m_\rho^2},\tag{61}$$

is not completely straightforward, since the coupling $g_{\omega\rho\pi}$ cannot be calculated on-shell. Nonetheless by extrapolating to the soft-pion limit (zero pion four-momentum) we can get a reasonable estimate for the strength at the pole in Eq. (61). The results for $g_{\omega\rho\pi}$ determined in this way are within 20% of the prediction of universal coupling, $g_{\omega\rho\pi} = g_{\omega\pi\gamma} g_\rho$. The results for the form factor plotted in Fig. 13 again show good agreement between the full calculation and the VMD approximation.

In the amplitude for the decay $a_1^\pm \rightarrow \pi^\pm \gamma$, the two-body diagram involves the terms in the nonlocal current $G_1(i\gamma_5 \otimes i\gamma_5)$ and $G_2(\gamma^\nu \gamma_5 \otimes \gamma_\nu \gamma_5)$ which have a type-II structure (10). Since the a_1 mass lies above the pseudo-threshold for parameter set B, in that case both the triangle and two-body diagrams require residue contributions. Gauge invariance imposes the following structure on the amplitude,

$$\langle \gamma(q_1) \pi^b(q_2) | a_1^a \rangle = i\epsilon^{ab3} e g_{a_1 \pi \gamma} \left[\epsilon_{a_1} \cdot \epsilon_\gamma^* + \frac{2(q_2 \cdot \epsilon_{a_1})(q_2 \cdot \epsilon_\gamma^*)}{(m_{a_1}^2 - m_\pi^2)} \right]. \quad (62)$$

The values calculated for $g_{a_1 \pi \gamma}$, and the corresponding decay widths, are presented in Table 5. With parameter set A the dressed scalar piece of the nonlocal photon coupling and the two-body diagrams make relatively small contributions; for set B, these pieces are rather larger in magnitude but largely cancel with each other. The final results for all choices of parameters are much smaller than the experimental measurement [63] of 640 ± 246 keV.

VII. CONCLUSIONS

We have investigated extended versions of the model proposed in Ref. [23] with nonlocal, four-fermion interactions, based on the separable form (4) suggested by instanton-liquid studies [14]. The interaction form factors ensure the convergence of all quark-loop integrals and, for most of the acceptable range of parameters, also lead to quark confinement [23]. The familiar problems of the NJL model are therefore eliminated whilst retaining much of the simplicity of that approach.

Quark confinement is particularly important in applying such a model to heavier mesons than the pion, since it avoids a threshold for $\bar{q}q$ production occurring at an inconveniently low energy, as in the NJL model. This feature of the nonlocal approach makes it especially well suited as the basis for the extended model that we study here, with interactions that bind vector and axial-vector mesons.

The analytic structure of the quark propagator, with poles at complex momenta, means that a scheme has to be specified for continuing amplitudes to Minkowski space. We have

used the scheme suggested by Lee and Wick [34] and Cutkosky *et al.* [35], which leads to nonanalytic behaviour of the meson propagators above a pseudo-threshold. This behaviour ensures that no poles appear in the longitudinal vector channels. It also provides restrictions on both the admissible range of model parameters and the region of applicability of the model.

In order to calculate the pion decay constant, which sets the basic scale for the model, as well as electromagnetic couplings, we need to construct conserved currents that are consistent with our nonlocal interaction. This has been done using the Noether-like method of Ref. [23]. Ward identities related to the current conservation follow automatically and several have been analytically checked, including the Gell-Mann–Oakes–Renner relation and the low-energy theorem for $\pi^0 \rightarrow \gamma\gamma$ in the chiral limit. The latter involves the axial anomaly, which has formed a long-standing problem for the usual NJL model with its cut-offs on the quark propagators.

Working at tree level in terms of mesons (leading order in $1/N_c$) and to all orders in momentum, we have calculated the meson masses and various strong decay rates. When the ρ mass is used to fix the strength of the relevant four-quark vertex, we find that the ρ -meson width is reasonably well described. In particular the model provides an improvement on the underestimated value obtained in the extended NJL model [48]. As in the NJL model, a light σ is found, with a mass similar to that found in a number of analyses of $\pi\pi$ scattering [45]. The calculated mass of the a_1 meson is somewhat lighter than the observed value. By cutting down the available phase-space, this also means that the model gives too small a width for the decay $a_1 \rightarrow \rho\pi$.

Various electromagnetic quantities have also been calculated in this model. The decay rates found in the model are in reasonably good agreement with the observed ones, except for the case of $a_1 \rightarrow \pi\gamma$. The electromagnetic form factor of the pion agrees well with the data, at least below the ρ pole. The form factors for $\gamma\gamma^* \rightarrow \pi$ and $\omega \rightarrow \pi\gamma^*$ are also in agreement with the, admittedly rather limited, data currently available. We have also compared our results for electromagnetic form factors with vector-dominance formulae using

on-shell couplings as calculated in the model. Although diagrams where the photon couples directly to the quarks make a significant contribution, they combine with diagrams that involve an intermediate vector meson to give results that are very close to those of VMD, at least at low momenta. The model is thus able to provide some support for the idea of vector dominance in photon-meson interactions.

Overall the level of agreement with observed meson properties is satisfactory, given the simple nature of the model and the fact that important effects have not been included at the current level of approximation. It is desirable to extend the current work to include meson-loop effects ($1/N_c$ corrections) since these could be significant, in particular for the ρ and a_1 mesons.

ACKNOWLEDGEMENTS

MCB acknowledges helpful discussions with W. Broniowski. This work is supported by the EPSRC and PPARC.

APPENDIX A: $\pi^0 \rightarrow \gamma\gamma$

We outline here the various contributions to the $\pi^0 \rightarrow \gamma\gamma$ amplitude in this model. We work in the chiral limit, where the axial anomaly requires that $g_{\pi\gamma\gamma} = \frac{1}{2}$. The relevant diagrams are shown in Fig. 11. Consider first the simpler case where vector meson degrees of freedom are not present in the model, setting $G_2 = G_3 = 0$. The triangle diagrams where both of the photons couple to the local current, γ_μ , contribute

$$4i\epsilon_{\alpha\beta\mu\nu}q_1^\alpha q_2^\beta\epsilon_1^{*\mu}\epsilon_2^{*\nu}e^2g_{\pi qq}\int\frac{d^4p}{(2\pi)^4}\frac{f^2(p)}{[p^2-m_0^2(p^2)]^3}\left(-2m_0(p^2)+4m_0'(p^2)\frac{(p\cdot q)^2}{q^2}\right. \\ \left.+4m_0'(p^2)\frac{[p\cdot(q_1-q_2)]^2}{(q_1-q_2)^2}\right), \quad (A1)$$

where the prime denotes a derivative with respect to p^2 . The contribution of diagrams where one of the photons couples to the nonlocal piece of the current, with a scalar loop insertion (35), is

$$4i\epsilon_{\alpha\beta\mu\nu}q_1^\alpha q_2^\beta\epsilon_1^{*\mu}\epsilon_2^{*\nu}e^2g_{\pi qq}\int\frac{d^4p}{(2\pi)^4}\frac{f^2(p)4m_0'(p^2)}{[p^2-m_0^2(p^2)]^3}\left(p^2-\frac{(p\cdot q)^2}{q^2}-\frac{[p\cdot(q_1-q_2)]^2}{(q_1-q_2)^2}\right). \quad (\text{A2})$$

Diagrams with a nonlocal coupling at both photon vertices do not contribute to the amplitude because the resulting Dirac trace vanishes. Converting the sum of (A1) and (A2) into Euclidean space, and changing variable to

$$t = \frac{m_0^2(p_E^2)}{p_E^2}, \quad (\text{A3})$$

leads to

$$-2\epsilon_{\alpha\beta\mu\nu}q_1^\alpha q_2^\beta\epsilon_1^{*\mu}\epsilon_2^{*\nu}\frac{\alpha_{EM}}{\pi}\frac{g_{\pi qq}}{m_0(0)}\int_0^\infty\frac{dt}{(1+t)^3}. \quad (\text{A4})$$

The low-energy theorem now follows by invoking the analogue of the Goldberger–Treiman relation [64] in this model,

$$g_{\pi qq} = \frac{m_0(0)}{f_\pi}, \quad (\text{A5})$$

which was derived in Ref. [23] by considering f_π in the chiral limit.³

In the extended model with vector mesons, $g_{\pi qq}$ is affected by the pseudoscalar-axial mixing induced by the G_2 coupling (28,29). However, the form of f_π is also modified, as discussed in Subsec. III D, and hence Eq.(A5) remains valid in the chiral limit [30]. In addition the photons are on-shell and so we need only consider the bare γqq vertex and the nonlocal piece (35) with a scalar one-quark loop, as also discussed in Subsec. III D. The sum of the contributions (A1) and (A2) therefore yields $g_{\pi\gamma\gamma} = \frac{1}{2}$, just as in the model without vector mesons.

This feature is in agreement with the analysis of Ref. [65], where it was shown that for a quark propagator without wave function renormalization, then the anomaly is saturated by taking only the leading part of the pion Bethe–Salpeter amplitude and the dressed γqq structures subject to the Ward identity for that vertex. The statement is non-trivial because

³In the notation of Ref. [23] $g_{\pi qq}$ is $Z_\pi^{\frac{1}{2}}$.

terms in the pion amplitude that are linear in momentum can contribute to the decay amplitude, even in the chiral limit. For instance, the $\not{q}\gamma_5$ term which appears in $V_\pi(q)$ for this model gives rise to additional triangle-diagram contributions. From such diagrams with two local photon vertices, one finds

$$4i\epsilon_{\alpha\beta\mu\nu}q_1^\alpha q_2^\beta\epsilon_1^{*\mu}\epsilon_2^{*\nu}e^2\frac{\tilde{g}_{\pi qq}}{m_\pi}\int\frac{d^4p}{(2\pi)^4}\frac{f^2(p)}{[p^2-m_0^2(p^2)]^3}\left(-2p^2-2m_0^2(p^2)+4\frac{(p\cdot q)^2}{q^2}+4\frac{[p\cdot(q_1-q_2)]^2}{(q_1-q_2)^2}\right). \quad (\text{A6})$$

Since $\tilde{g}_{\pi qq}$ is of $\mathcal{O}(m_\pi)$ in the chiral expansion, this expression is of $\mathcal{O}(1)$. Similar diagrams with one local and one nonlocal vertex give

$$4i\epsilon_{\alpha\beta\mu\nu}q_1^\alpha q_2^\beta\epsilon_1^{*\mu}\epsilon_2^{*\nu}e^2\frac{\tilde{g}_{\pi qq}}{m_\pi}\int\frac{d^4p}{(2\pi)^4}\frac{f^2(p)8m_0(p^2)m_0'(p^2)}{[p^2-m_0^2(p^2)]^3}\left(p^2-\frac{(p\cdot q)^2}{q^2}-\frac{[p\cdot(q_1-q_2)]^2}{(q_1-q_2)^2}\right). \quad (\text{A7})$$

(The diagrams with two nonlocal vertices again have a vanishing Dirac trace.)

Since the sum of (A6) and (A7) is non-zero, there must be some contribution that cancels them in the full amplitude for the anomalous process. The relevant piece arises from the two-body diagram, which is displayed in Fig. 11. Terms in the nonlocal vector current of the form $G_2(\gamma^\nu\gamma_5 \otimes \gamma_\nu\gamma_5)$ with a type-I (8) structure are responsible for the $\gamma qqqq$ vertex. (Note that for simplicity we have suppressed isospin factors.) This diagram factorizes into two separate loop integrals, the loop between the two photons giving rise to the $\epsilon_{\alpha\beta\mu\nu}$ factor. The other loop is simply a linear combination of the familiar integrals $J_{AP}(m_\pi^2)$ and $J_{AA}^L(m_\pi^2)$ from Subsec. III B. This combination can be simplified by recalling the definitions of the pion-quark coupling constants in (28). In the chiral limit, the contribution of this diagram can be written as

$$4i\epsilon_{\alpha\beta\mu\nu}q_1^\alpha q_2^\beta\epsilon_1^{*\mu}\epsilon_2^{*\nu}e^2\frac{\tilde{g}_{\pi qq}}{m_\pi}\int\frac{d^4p}{(2\pi)^4}\frac{4f(p)f'(p)}{[p^2-m_0^2(p^2)]^2}\left(p^2-\frac{(p\cdot q)^2}{q^2}-\frac{[p\cdot(q_1-q_2)]^2}{(q_1-q_2)^2}\right). \quad (\text{A8})$$

Converting to Euclidean space and integrating by parts, this expression can be shown to cancel exactly with the sum of (A6) and (A7), demonstrating that the low-energy theorem for $\pi^0 \rightarrow \gamma\gamma$ holds in the extended model.

[1] Y. Nambu and G. Jona-Lasinio, Phys. Rev. **122** (1961) 345; **124** (1961) 246.

[2] U. Vogl and W. Weise, Prog. Part. Nucl. Phys. **27** (1991) 195; S. P. Klevansky, Rev. Mod. Phys. **64** (1992) 649; T. Hatsuda and T. Kunihiro, Phys. Rep. **247** (1994) 221.

[3] J. Bijnens, Phys. Rep. **265** (1996) 369.

[4] J. Bijnens, E. de Rafael and H. Zheng, Z. Phys. **C62** (1994) 437.

[5] J. Bijnens and J. Prades, Phys. Lett. **B320** (1994) 130; Z. Phys. **C64** (1994) 475.

[6] T. Meissner, E. Ruiz Arriola and K. Goeke, Z. Phys. **A336** (1990) 91.

[7] R. S. Willey, Phys. Rev. **D48** (1993) 2877; T. Gherghetta, Phys. Rev. **D50** (1994) 5985.

[8] E. Nikolov, W. Broniowski, C. V. Christov, G. Ripka and K. Goeke, Nucl. Phys. **A608** (1996) 411.

[9] C. Schüren, F. Döring, E. Ruiz Arriola and K. Goeke, Nucl. Phys. **A565** (1993) 687.

[10] R. Alkofer, H. Reinhardt, H. Weigel and U. Zuckert, Phys. Lett. **B298** (1992) 132; U. Zuckert, R. Alkofer, H. Reinhardt and H. Weigel, Nucl. Phys. **A570** (1994) 445.

[11] E. Ruiz Arriola and L. L. Salcedo, Phys. Lett. **B316** (1993) 148; Nucl. Phys. **A590** (1995) 703.

[12] I. J. R. Aitchison and G. Ripka, Nucl. Phys. **A606** (1996) 292.

[13] R. Alkofer and P. A. Amundsen, Nucl. Phys. **B306** (1988) 305; A. A. Bel'kov, D. Ebert and A. V. Emelyanenko, Nucl. Phys. **A552** (1993) 523; K. Langfeld, C. Kettner and H. Reinhardt, Nucl. Phys. **A608** (1996) 331; T. Hamazaki and T. Kugo, Prog. Theor. Phys. **92** (1994) 645.

[14] D. I. Dyakonov and V. Yu. Petrov, Nucl. Phys. **B245** (1984) 259; Sov. Phys. JETP **62** (1985) 204, 431; Nucl. Phys. **B272** (1986) 457.

[15] H. Ito, W. W. Buck and F. Gross, Phys. Lett. **B248** (1990) 28; Phys. Rev. **C43** (1991) 2483; Phys. Rev. **C45** (1992) 1918.

[16] S. Schmidt, D. Blaschke and Y. L. Klavinovsky, Phys. Rev. **C50** (1994) 435.

[17] G. V. Efimov and M. A. Ivanov, *The Quark Confinement Model of Hadrons* (IOP, Bristol and Philadelphia, 1993); G. V. Efimov and S. N. Nedelko, Phys. Rev. **D51** (1995) 176; Ja. V. Burdanov, G. V. Efimov, S. N. Nedelko and S. A. Solunin, Phys. Rev. **D54** (1996) 4483.

[18] K. Langfeld and M. Rho, Nucl. Phys. **A596** (1996) 451.

[19] H. Reinhardt, Phys. Lett. **B257** (1991) 375; K. Langfeld and M. Schaden, Phys. Lett. **B272** (1991) 100; K. Langfeld, R. Alkofer and H. Reinhardt, Phys. Lett. **B277** (1992) 163.

[20] P. T. Cahill and C. D. Roberts Phys. Rev. **D32** (1985) 2419; J. Praschifka, C. D. Roberts and R. T. Cahill, Phys. Rev. **D36** (1987) 209.

[21] M. R. Frank and C. D. Roberts, Phys. Rev. **C53** (1996) 390.

[22] C. D. Roberts and A. G. Williams, Prog. Part. Nucl. Phys. **33** (1994) 477.

[23] R. D. Bowler and M. C. Birse, Nucl. Phys. **A582** (1995) 655.

[24] M. Buballa and S. Krewald, Phys. Lett. **B294** (1992) 19.

[25] V. Bernard and U.-G. Meissner, Nucl. Phys. **A489** (1988) 647.

[26] M. Wakamatsu and W. Weise, Z. Phys. **A331** (1988) 173; D. Ebert and H. Reinhardt, Nucl. Phys. **B271** (1986) 188; J. Bijnens, C. Bruno and E. de Rafael, Nucl. Phys. **B390** (1993) 501; J. Prades, Z. Phys. **C63** (1994) 491; E. Ruiz Arriola, Phys. Lett. **B253** (1991) 430.

[27] S. Klimt, M. Lutz, U. Vogl and W. Weise, Nucl. Phys. **A516** (1990) 429, 469.

[28] V. Bernard, R. L. Jaffe and U.-G. Meissner, Nucl. Phys. **B308** (1988) 753.

[29] G. 't Hooft, Phys. Rev. Lett. **37** (1976) 8; Phys. Rev. **D14** (1976) 3432.

[30] R. S. Plant, unpublished.

[31] M. Gell-Mann, R. Oakes and B. Renner, Phys. Rev. **175** (1968) 2195.

[32] M. Stingl, Phys. Rev. **D34** (1986) 3863; **D36** (1987) 651 (E); U. Häbel, R. Königning, H.-G. Reusch, M. Stingl and S. Wigard, Z. Phys. **A336** (1990) 435.

[33] C. Savkli and F. Tabakin, hep-ph/9702251 (1997).

[34] T. D. Lee and G. C. Wick, Nucl. Phys. **B9** (1969) 209.

[35] R. E. Cutkosky, P. V. Landshoff, D. I. Olive and J. C. Polkinghorne, Nucl. Phys. **B12** (1969) 281.

[36] U.-G. Meissner, Phys. Reports **161** (1988) 213.

[37] M. C. Birse, Z. Phys. **A335** (1996) 231.

[38] W. Broniowski, G. Ripka, E. Nikolov and K. Goeke, Z. Phys. **A354** (1996) 421.

[39] C. D. Roberts, Nucl. Phys. **A605** (1996) 475; R. Alkofer, A. Bender and C. D. Roberts, Int. J. Mod. Phys. **A10** (1995) 3319; C. J. Burden, C. D. Roberts and M. J. Thompson, Phys. Lett. **B371** (1996) 163; P. C. Tandy, Prog. Part. Nucl. Phys. **36** (1996) 37; C. D. Roberts, R. T. Cahill, M. E. Sevior and N. Iannella, Phys. Rev. **D49** (1994) 125.

[40] D. Kekez and D. Klabučar, Phys. Lett. **B387** (1996) 14.

[41] M. R. Frank, K. L. Mitchell, C. D. Roberts and P. C. Tandy, Phys. Lett. **B359** (1995) 17.

[42] J. Ball and T. Chiu, Phys. Rev. **D22** (1980) 2542.

[43] M. A. Shifman, A. I. Vainshtein and V. I. Zakharov, Nucl. Phys. **B147** (1979) 385, 448, 519.

[44] J. Gasser and H. Leutwyler, Phys. Rep. **87** (1982) 77.

[45] S. Ishida, M. Y. Ishida, H. Takahashi, T. Ishida, K. Takamatsu and T. Tsuru, Prog. Theor. Phys. **95** (1996) 745; B. S. Zou and D. V. Bugg, Phys. Rev. **D50** (1994) 591; N. A. Tornqvist

and M. Roos, Phys. Rev. Lett. **76** (1996) 1575; M. Harada, F. Sannino and J. Schechter, Phys. Rev. **D54** (1996) 1991.

[46] Particle Data Group, Phys. Rev. **D54** (1996) 1.

[47] C. J. Burden, L. Qian, C. D. Roberts, P. C. Tandy and M. J. Thomson, Austr. J. Phys. **50** (1997) 95.

[48] V. Bernard, A. H. Blin, B. Hiller, U.-G. Meissner and M. C. Ruivo, Phys. Lett. **B305** (1993) 163; A. Polleri, R. A. Broglia, P. M. Pizzochero and N. N. Scoccola, hep/ph 9611300 (1996).

[49] S. Coleman, J. Wess and B. Zumino, Phys. Rev. **177** (1969) 2239; C. G. Callan, S. Coleman, J. Wess and B. Zumino, Phys. Rev. **177** (1969) 2247.

[50] H. Albrecht et al., Z. Phys. **C58** (1993) 61.

[51] S. Weinberg, Phys. Rev. Lett. **18** (1967) 507.

[52] S. R. Amendolia et al., Nucl. Phys. **B277** (1986) 168.

[53] C. N. Brown et al., Phys. Rev. **D8** (1973) 92; C. J. Bebek et al., Phys. Rev. **D9** (1974) 1229.

[54] L. M. Barkov et al., Nucl. Phys. **B256** (1985) 365; I. B. Vasserman et al., Sov. J. Nucl. Phys. **33** (1981) 709; L. M. Barkov et al., Novosibirsk preprint INP 79-69 (1979); G. Cosme et al., ORSAY preprint LAL-1287 (1976); A. Quenzer et al., Phys. Lett. **B76** (1978) 512; S. R. Amendolia et al., Phys. Lett. **B138** (1984) 454.

[55] V. Bernard and U.-G. Meissner, Phys. Rev. Lett. **61** (1988) 2296.

[56] H.-J. Behrend et al., Z. Phys. **C49** (1991) 401.

[57] D. Dale and A. Gasparian (spokespersons), Jefferson Lab letter of intent LOI-96-002.

[58] S. I. Eidelman, *The DAΦNE Physics Handbook*, eds. L. Maiani, G. Pancheri and N. Paver (INFN, Frascati, 1995), p. 499.

[59] R. I. Dzhelyadin et al., Phys. Lett. **B102** (1981) 296.

[60] M. Bando and M. Harada, Phys. Rev. **D49** (1994) 6096 ; G. Köpp, Phys. Rev. **D10** (1974) 932.

[61] L. G. Landsberg, Phys. Rep. **128** (1985) 301.

[62] F. Klingl, N. Kaiser and W. Weise, hep/ph 9607431 (1996).

[63] M. Zielinski et al., Phys. Rev. Lett. **52** (1984) 1195.

[64] M. Goldberger and S. Treiman, Phys. Rev. **110** (1958) 1178.

[65] M. Bando, M. Harada and T. Kugo, Prog. Theor. Phys. **91** (1994) 927.

APPENDIX: TABLES

Parameter	Set A	Set B	Parameter	Set A	Set B
$m_0(0)(\text{MeV})$	280	320	$m(0)(\text{MeV})$	326	370
$m_c(\text{MeV})$	8.4	11.0	$\Lambda(\text{MeV})$	995	846
$G_1(\text{GeV}^{-2})$	37.1	57.6	$G_2(\text{GeV}^{-2})$	-5.70	-6.53
$G_3(\text{GeV}^{-2})$	-5.20	-5.86	$G_4(\text{GeV}^{-2})$	-0.80	-4.14
$G_5(\text{GeV}^{-2})$	2.57	4.76	r	0.87	0.88

Table 1. Values of the model parameters for sets A and B, fitted as discussed in the text.

Also shown are the dynamical quark mass and the GMOR ratio (47).

Set A	Set B
$\pm 496 \pm 130i$	$\pm 404 \pm 257i$
$\pm 1168 \pm 790i$	$\pm 962 \pm 702i$
$\pm 1488 \pm 1155i$	$\pm 1242 \pm 1005i$
$\pm 1742 \pm 1436i$	$\pm 1463 \pm 1240i$

Table 2. Positions of the lowest four sets of poles in the quark propagator.

Particle	Set A			Set B		
	Mass	g_{iqq}	\tilde{g}_{iqq}	Mass	g_{iqq}	\tilde{g}_{iqq}
π	Fit	3.44	0.0739	Fit	3.91	0.0715
σ	443.2	3.51	–	465.8	4.06	–
ρ	Fit	1.12	–	Fit	1.11	–
a_1	946.8	1.13	–	1061.5	2.27	–
ω	Fit	1.07	–	Fit	1.05	–
f_1	Fit	0.89	–	Fit	2.51	–
a_0	Fit	0.75	–	Fit	1.71	–
η^*	874.9	0.83	0.190	899.4	2.36	1.448

Table 3. Meson masses (in MeV) and couplings of the mesons to quarks. The couplings g_{iqq} and \tilde{g}_{iqq} are defined by the equations (27) and (28).

Coupling	Set A		Set B	
	Value	Width(MeV)	Value	Width(MeV)
$g_{\sigma\pi\pi}(\text{MeV})$	1438	108.0	1625	135.1
$g_{\rho\pi\pi}$	5.52	126.0	5.26	114.0
$g_{a_1\sigma\pi}$	10.65	74.0	11.77	116.4
$g_{a_1\rho\pi}(\text{MeV})$	2174	44.0	4604	376.2
$h_{a_1\rho\pi}(\text{GeV}^{-1})$	18.19	–	10.87	–
R	–0.048	–	–0.087	–

Table 4. The meson couplings, as defined in equation (48), together with the corresponding partial widths. R is the ratio of the d - to s -wave amplitudes defined in (49).

	Set A	Set B		Set A	Set B
Quantity	Value	Value	Quantity	Value	Value
$g_{\rho\gamma}(\text{GeV}^2)$	0.0889	0.0773	g_ρ	6.67	7.67
$g_{\omega\gamma}(\text{GeV}^2)$	0.0308	0.0265	g_ω	19.92	23.12
$\langle r_\pi^2 \rangle(\text{fm}^2)$	0.346	0.344	—	—	—
$g_{\pi\gamma\gamma}$	0.505	0.501	—	—	—
$g_{\omega\pi\gamma}(\text{GeV}^{-1})$	-2.29	-2.25	$\Gamma(\omega \rightarrow \pi\gamma)(\text{keV})$	692	669
$g_{\rho\pi\gamma}(\text{GeV}^{-1})$	-0.755	-0.707	$\Gamma(\rho \rightarrow \pi\gamma)(\text{keV})$	71.6	62.7
$g_{a_1\pi\gamma}(\text{MeV})$	140.2	201.5	$\Gamma(a_1 \rightarrow \pi\gamma)$ (keV)	24.7	45.7

Table 5. Electromagnetic couplings of mesons.

APPENDIX: FIGURES

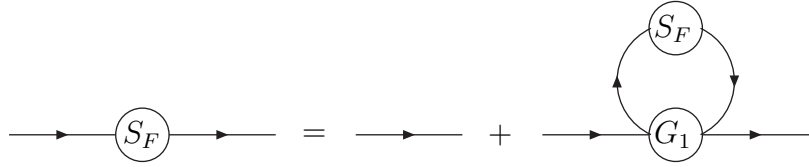


Fig. 1. Schwinger–Dyson equation for the quark propagator in the ladder approximation.

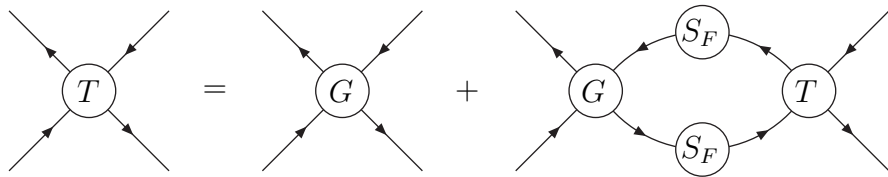


Fig. 2. Bethe–Salpeter equation for $\bar{q}q$ scattering in the ladder approximation.

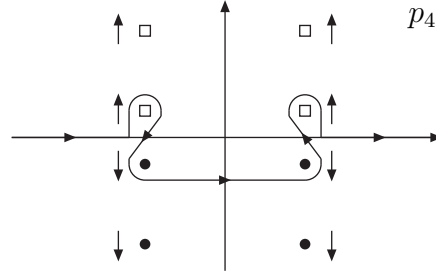


Fig. 3. Deformed integration contour in p_4 plane, beyond the pinch point. The open boxes denote the poles of the p_- propagator and the filled circles those of the p_+ propagator. The arrows indicate the directions in which these poles move as q_0 increases.



Fig. 4. Coupling of particle to an external current. V denotes the vertex function (25).

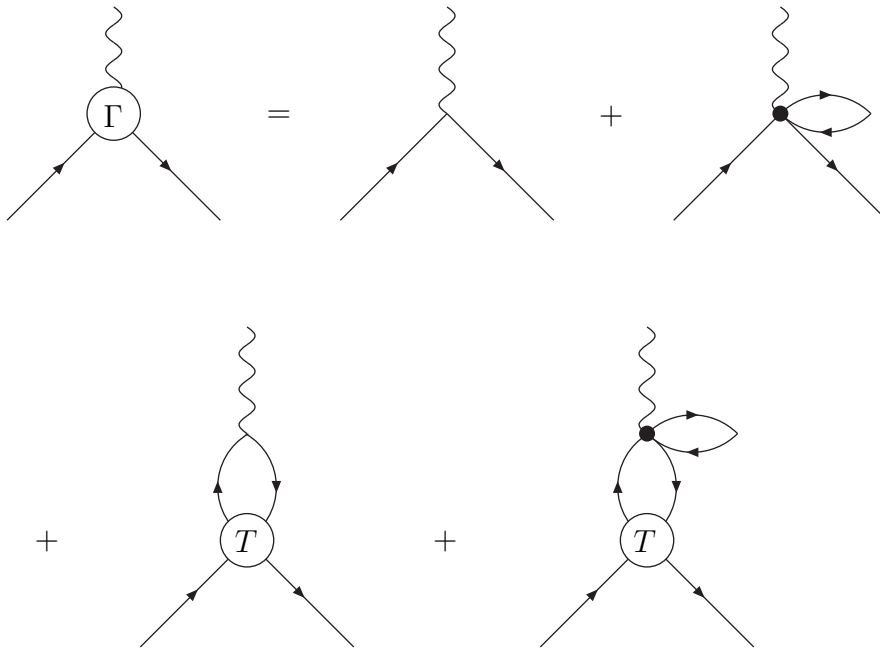


Fig. 5. The dressed $\gamma\bar{q}q$ vertex. T denotes the $\bar{q}q$ scattering matrix in either the transverse or longitudinal vector channel.

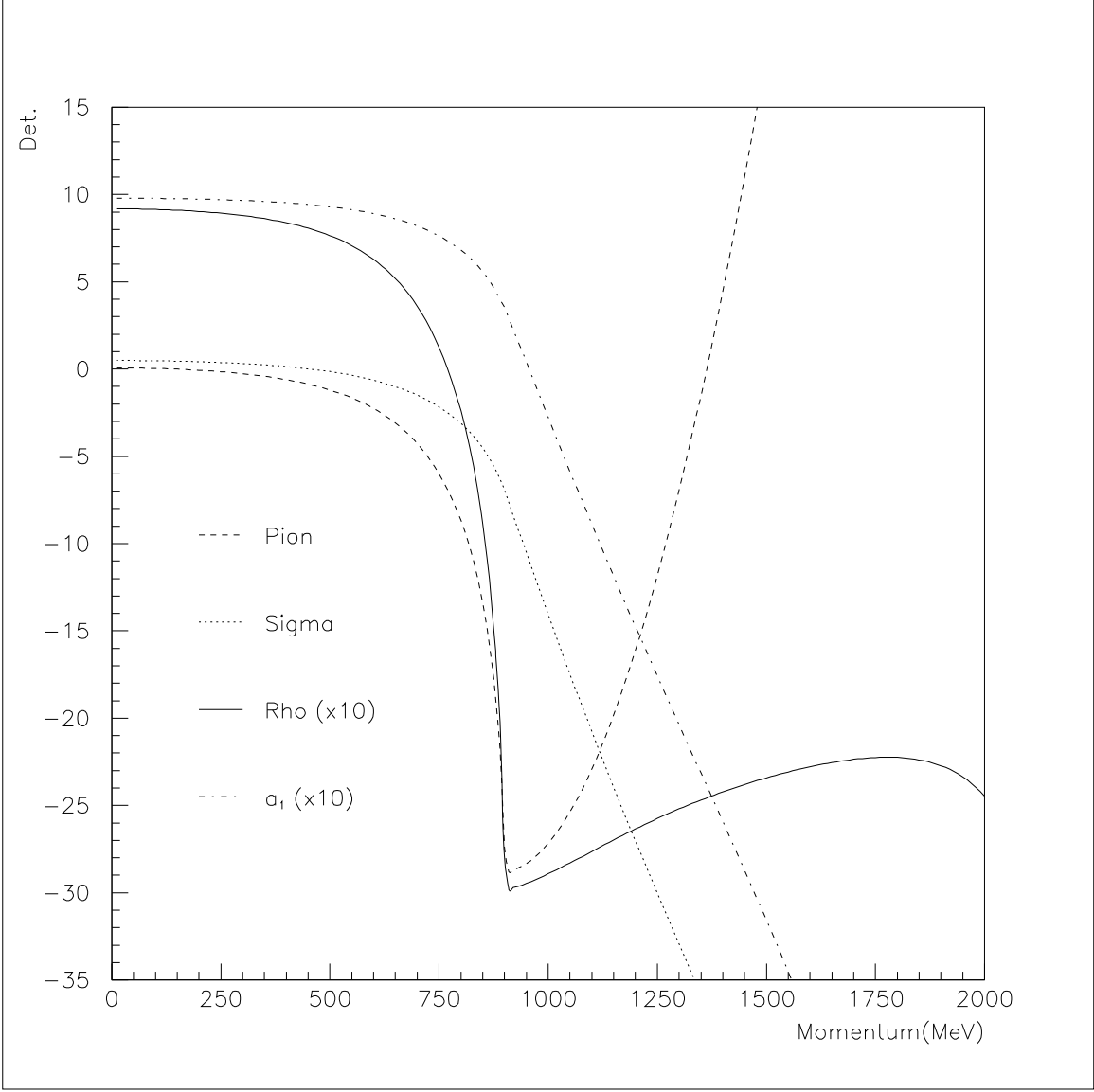


Fig. 6. Denominator of the propagator in the sigma channel, $1 - G_1 J_{SS}$, and the pion determinant, (29), as functions of the timelike meson momentum. The denominators of the ρ and a_1 propagators, $1 - G_2 J_{VV,AA}^T(q)$, are also displayed, scaled by a factor of 10.

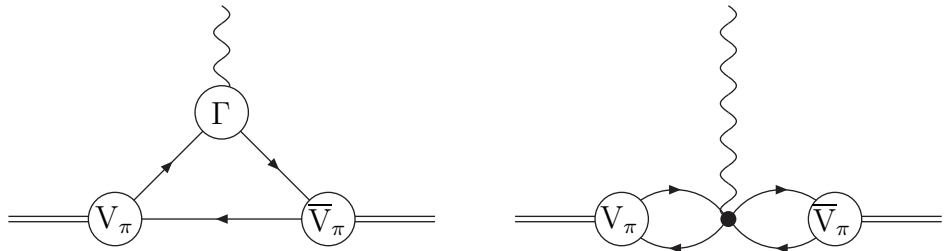


Fig. 7. Spacelike pion form factor. There is another similar triangle diagram where the photon couples to the anti-quark.

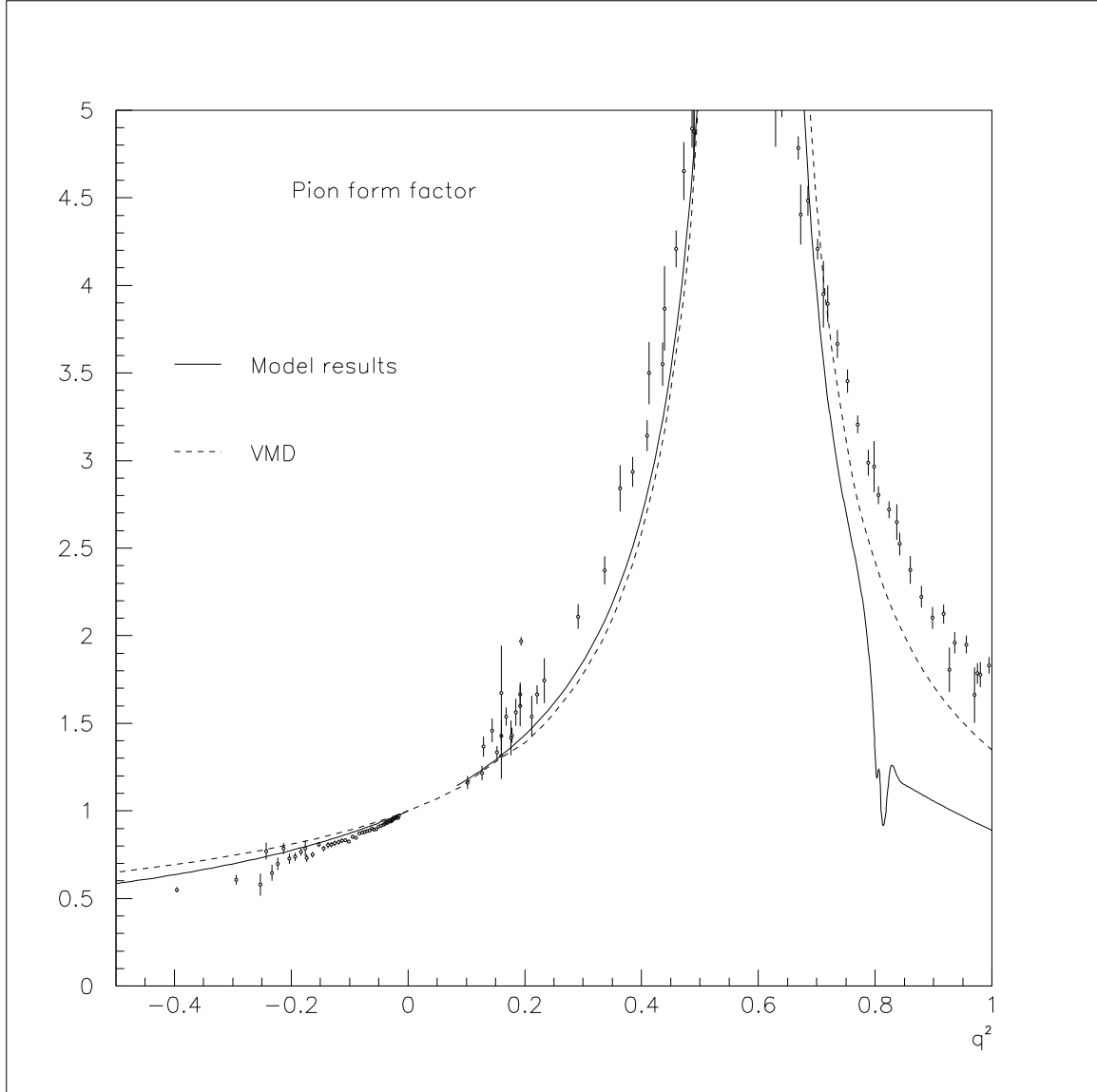


Fig. 8. Absolute value of the pion form factor, plotted against q^2 in GeV^2 . The solid line is the model result; the dashed line is the VMD approximation to it. The data points are from Refs. [52–54].

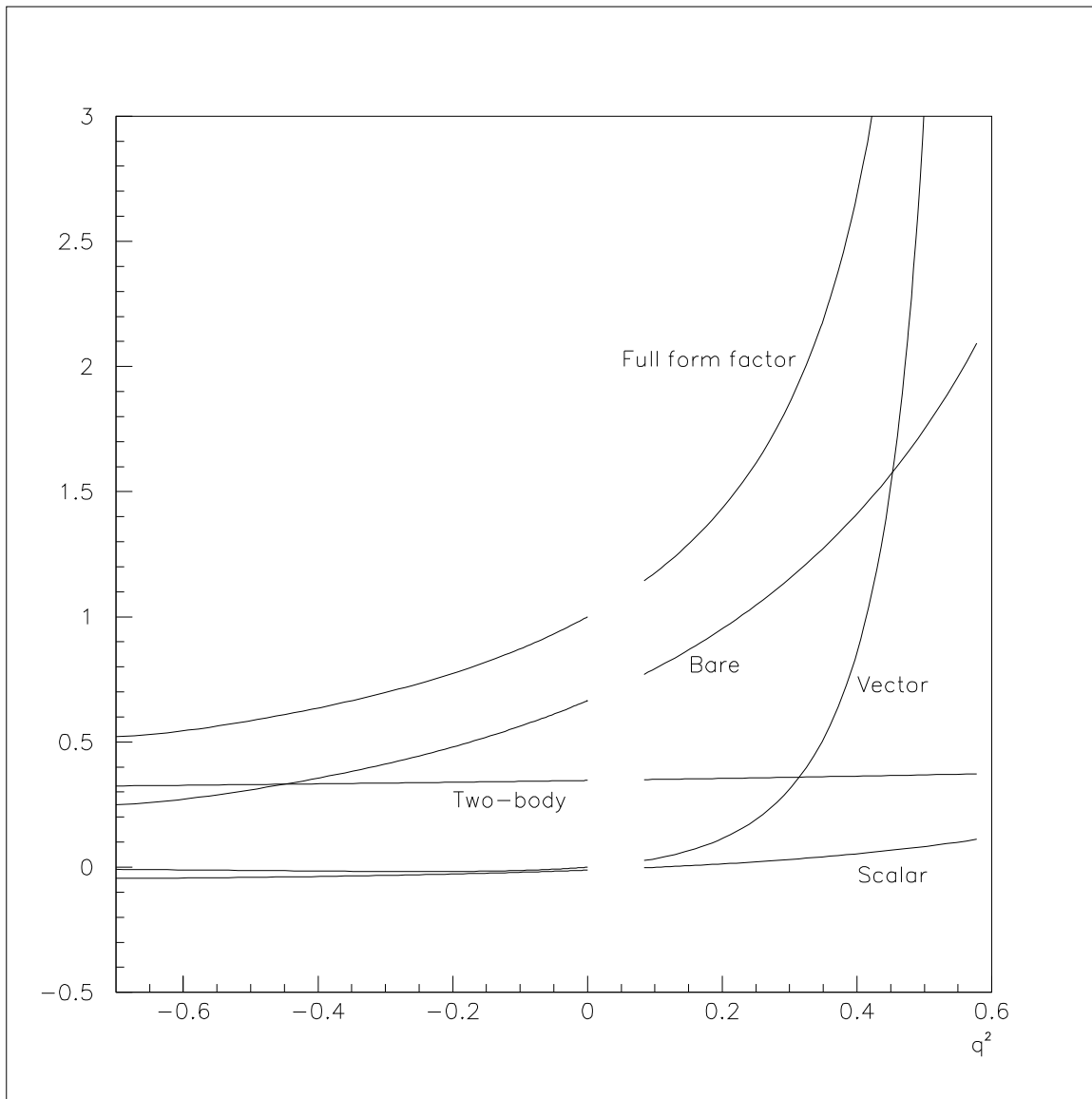


Fig. 9. Various contributions to the pion form factor, below the ρ pole, plotted against q^2 in GeV^2 . The different contributions are defined in the text.

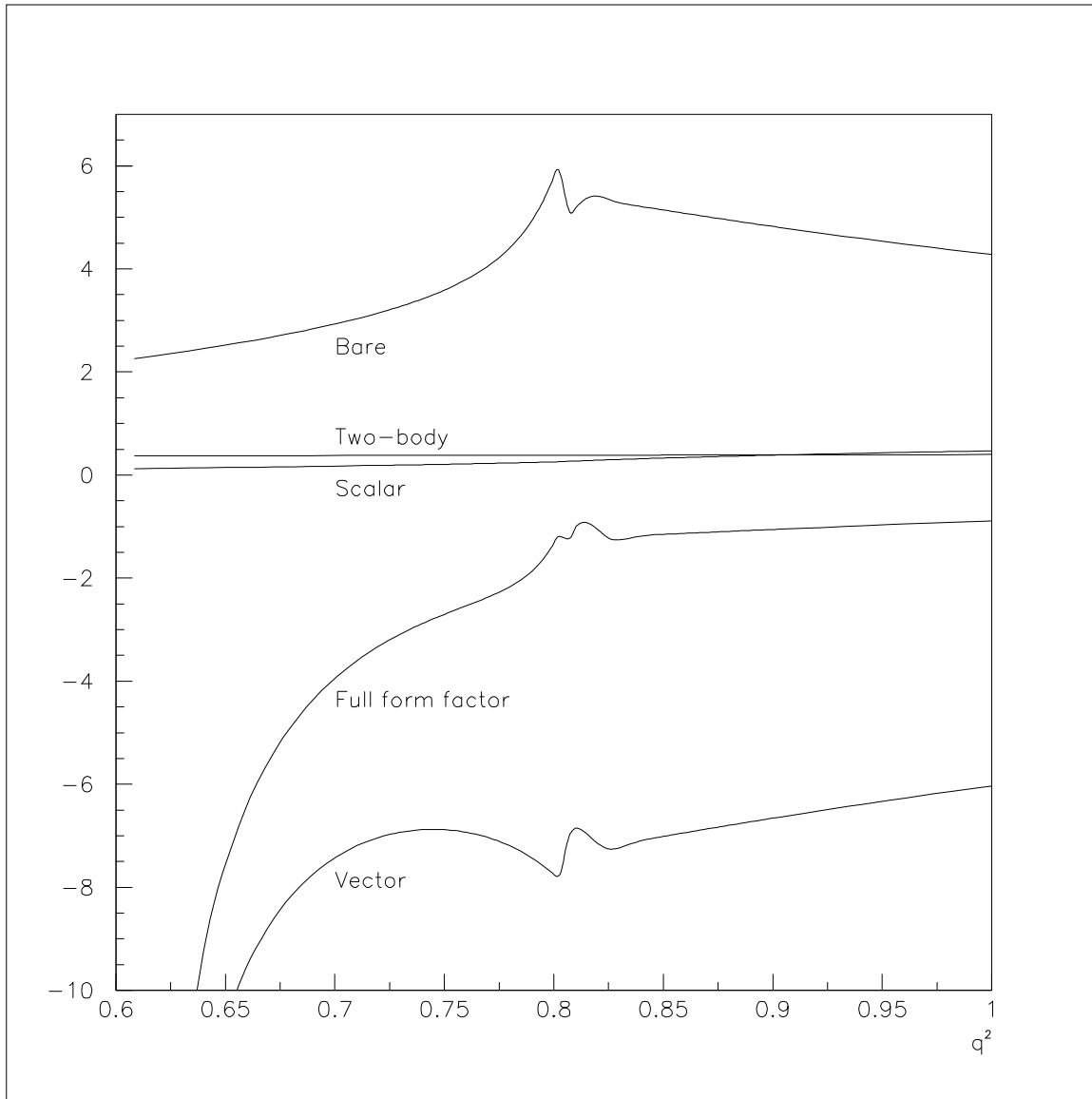


Fig. 10. Various contributions to the timelike pion form factor, above the ρ pole, plotted against q^2 in GeV^2 . The different contributions are defined in the text.

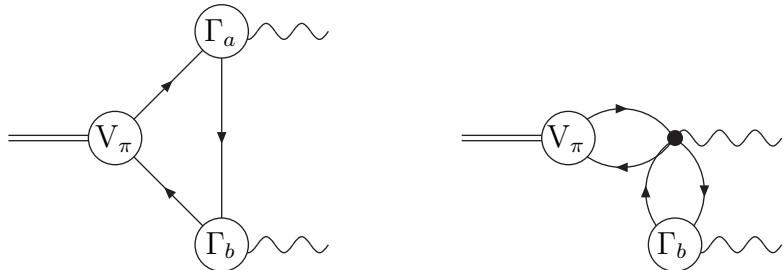


Fig. 11. $\pi^0 \rightarrow \gamma\gamma$. There are also similar diagrams with $a \leftrightarrow b$.

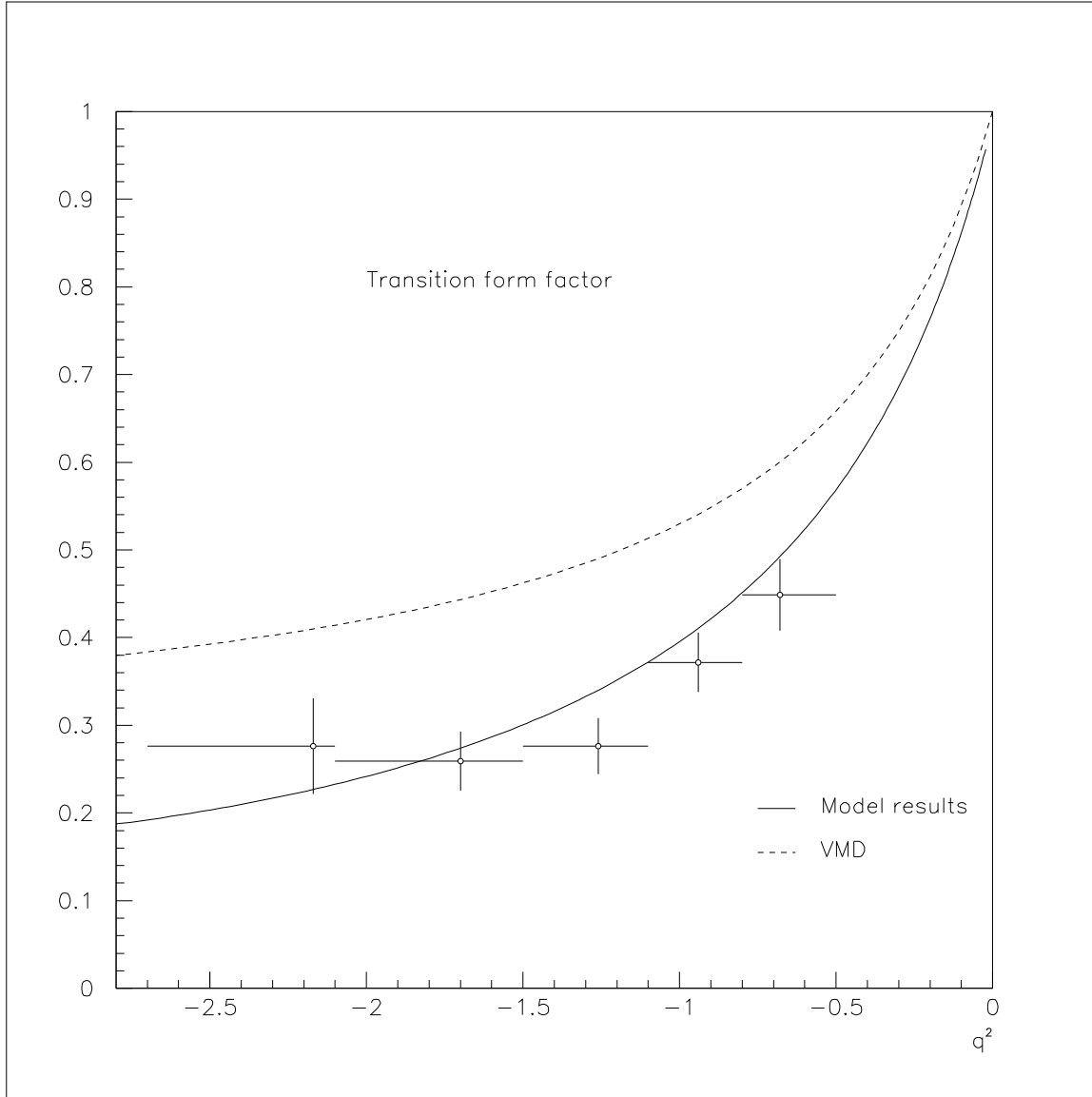


Fig. 12. The $\pi\gamma\gamma^*(q^2)$ transition form factor, plotted against q^2 in GeV^2 . The solid line is the model result; the dashed line is the VMD approximation to it. The data points are from Ref. [56].

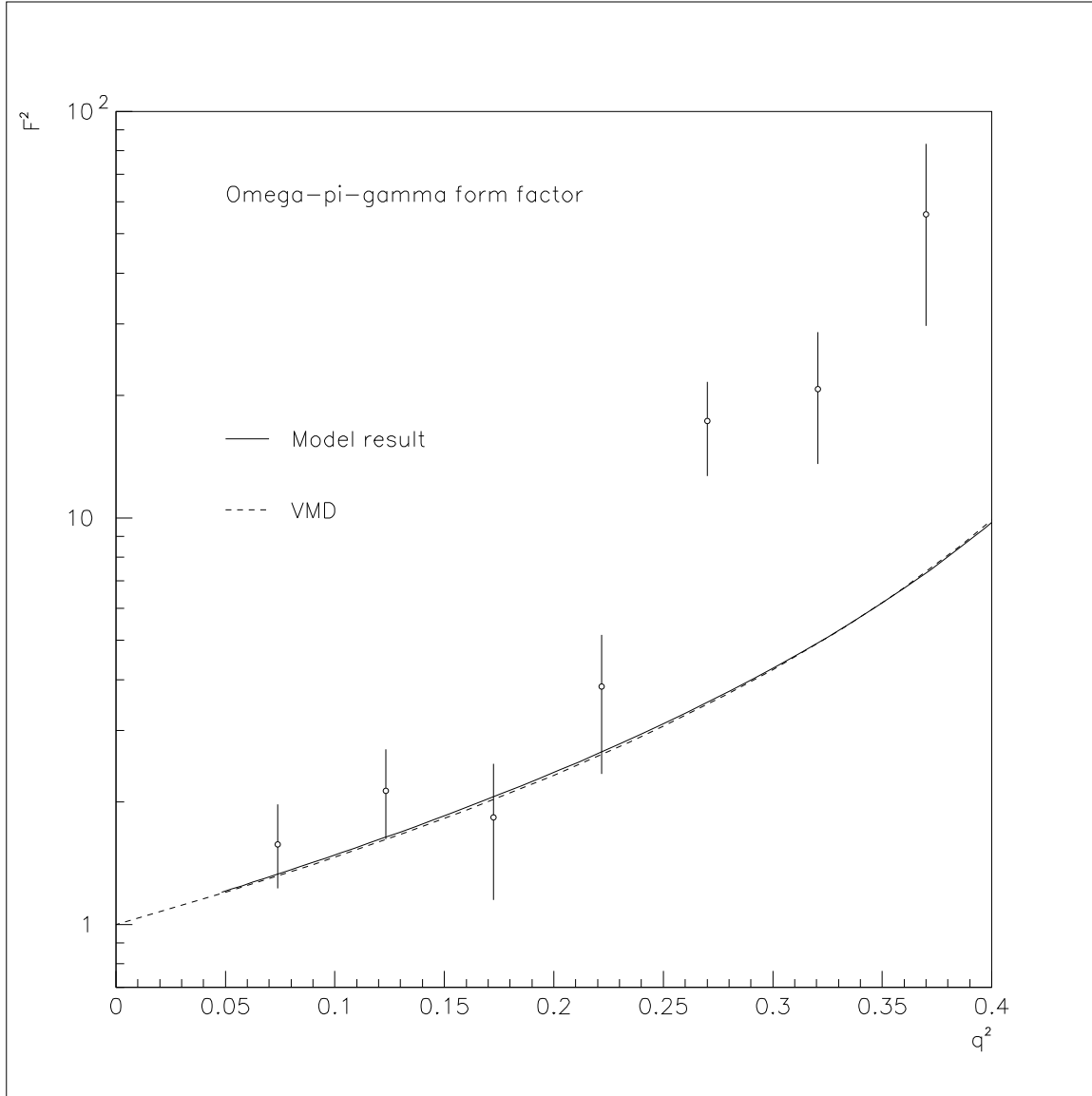


Fig. 13. The square of the $\omega\pi\gamma^*(q^2)$ form factor, plotted on a logarithmic scale against q^2 in GeV^2 . The solid line is the model result; the dashed line is the VMD approximation to it. The data points are from Ref. [59].